energy&fuels



pubs.acs.org/EF
Article

# Synthesis and Structure–Property Relationship of *meso*-Substituted Porphyrin- and Benzoporphyrin–Thiophene Conjugates toward Electrochemical Reduction of Carbon Dioxide

*Published as part of Energy & Fuels virtual special issue "Celebrating Women in Energy Research".*

H. Seelajaroen, D. H. Apaydin, B. Spingler, S. Jungsuttiwong, Y. Wongnongwa, R. Rojanathanes, N. S. Sariciftci, and P. Thamyongkit*

Cite This: *Energy Fuels* 2024, 38, 16555–16569

Read Online

ACCESS | Metrics & More | Article Recommendations | Supporting Information

**ABSTRACT:** A novel series of $Zn^{II}$-*trans*-$A_2B_2$ porphyrins and benzoporphyrins bearing phenyl and thiophene-based *meso*-substituents was successfully synthesized and characterized by spectroscopic and electrochemical techniques. Systematic comparison among the compounds in this series, together with the corresponding $A_4$ analogs previously studied by our group, led to the understanding of the effects of $\pi$-conjugated system extension of a porphyrin core through $\beta$-fused rings, replacement of the phenyl with the thiophene-based *meso*-groups, and introduction of additional thiophene rings on thienyl substituents on photophysical and electrochemical properties. Oxidative electropolymerization through bithiophenyl units of both $A_4$ and *trans*-$A_2B_2$ analogs was achieved, resulting in porphyrin– and benzoporphyrin–oligothiophene conjugated polymers, which were characterized by cyclic voltammetry and absorption spectrophotometry. Preliminary studies on catalytic performance toward electrochemical reduction of carbon dioxide ($CO_2$) was described herein to demonstrate the potential of the selected compounds for serving as homogeneous and heterogeneous electrocatalysts for the conversion of $CO_2$ to carbon monoxide (CO).

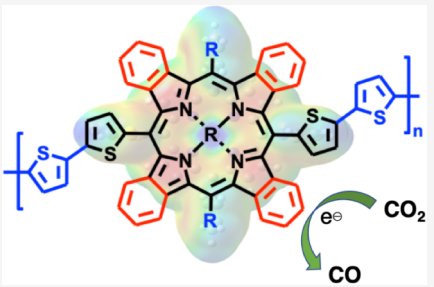


## 1. INTRODUCTION

Concern of the continuous increase in atmospheric carbon dioxide ($CO_2$) concentration emitted from fossil fuels has been growing during the past decades. $CO_2$ is also known to be one of the causes of global warming. With the abundance of $CO_2$, it can be used as a potential raw material in several industrial processes.[1] Therefore, capture and conversion of $CO_2$ to value-added products[2] such as CO, formic acid, methanol, ethanol, and ethylene, has attracted lots of interest. Conversion of $CO_2$ can be achieved through thermochemical,[3] biochemical,[4] photo(electro)chemical,[5−10] and electrochemical[11−17] approaches using either homogeneous or heterogeneous catalysts. Electrochemical reduction of $CO_2$ is a very practical option as this method can be operated under ambient conditions with the possibility to exploit renewable energy to drive the process.[18,19] A challenge of this approach is based on the fact that $CO_2$ is a highly stable molecule and thus requires a large energy input to be transformed into other products; for example, a one-electron reduction process of linear $CO_2$ to bent $CO_2^{\bullet-}$ requires a very high potential of −1.90 V vs normal hydrogen electrode (NHE) at pH 7 (eq 1) and, thus, considered a rate-determining step in an electrochemical conversion of $CO_2$.[20] Under an aprotic condition, $CO_2^{\bullet-}$ can undergo disproportionation and dimerization to form carbon monoxide (CO), carbonate ion ($CO_3^{2-}$), and oxalate ($C_2O_4^{2-}$) as proposed by previous studies.[21−23] Other possible pathways requiring substantially lower energy, compared to the above-mentioned one-electron process, such as reduction of $CO_2$ to CO involving 2 electrons and 2 protons are shown in eq 2.[24] However, an actual redox potential is higher than a thermodynamically formed potential due to the overpotential, and therefore, electrocatalysts are required.

$$CO_2 + e^- \rightarrow CO_2^- \quad E^{\circ\prime} = -1.90\text{V} \tag{1}$$

$$CO_2 + 2H^+ + 2e^- \rightarrow CO + H_2O \quad E^{\circ\prime} = -0.53\text{V} \tag{2}$$

Several kinds of the electrocatalysts, including metals,[25−28] metal oxides,[29−34] chalcogenides,[35,36] and organometallic compounds,[11,13,37−41] have been developed for catalyzing the reduction of $CO_2$. Among various types of the electrocatalysts, porphyrin-based complexes are one of the most attractive molecular catalysts due to well-developed synthesis, chemical

Received: April 17, 2024
Revised: June 12, 2024
Accepted: June 14, 2024
Published: August 26, 2024

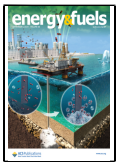





https://doi.org/10.1021/acs.energyfuels.4c01824
*Energy Fuels* 2024, 38, 16555−16569

stability, and molecular-level structural modification through variation of peripheral substituents and the central metal.[42] The reported studies show possibilities using metalloporphyrins as the electrocatalysts in both homogeneous and heterogeneous catalytic systems.[16,38,43−48] In the case of the homogeneous one, catalytic molecules are in the same phase as where the chemical reaction takes place; the catalytic sites are therefore well-defined. However, since the catalysts are dissolved in solution, the separation from the reaction phase and the regeneration after use are difficult. Additionally, low diffusion and mass transport of the catalysts might be an issue.[49] To overcome these drawbacks, heterogeneous electrocatalysis, where the catalysts are directly addressed on the electrode surface either by adsorption or covalent bonding, has been intensively studied.[49,50] Nevertheless, the heterogeneous molecular catalysts generally showed lower catalytic activity due to lower conductivity and limited accessibility of the catalytic sites than the homogeneous cases.

One of the approaches to immobilize the molecular catalysts on the electrode surface is electropolymerization of the catalysts.[51] In this way, introduction of polymerizable unit(s) on the catalyst molecules is required. Thiophene and its derivatives are promising units due to good charge transfer and stability of their conjugated polymers.[52,53] According to our previous studies, porphyrin (**ZnP-1** and **ZnP-2**, Chart 1) and

**Chart 1. Structures of Porphyrin and Benzoporphyrin Derivatives of Interest**

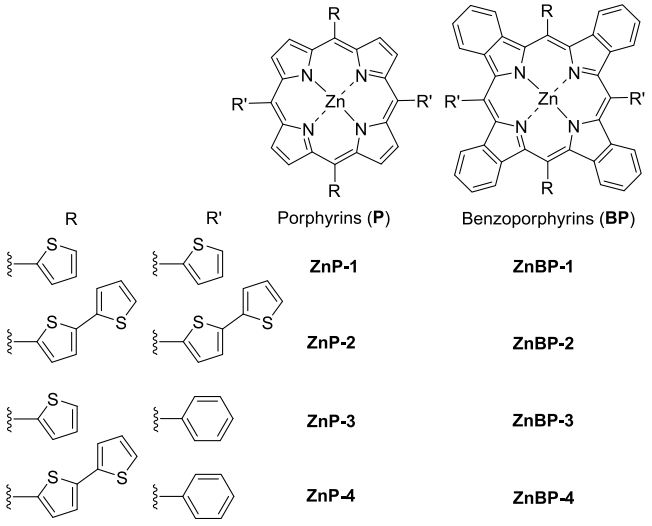


benzoporphyrin compounds bearing 4 identical thiophene-based *meso*-groups (**ZnBP-1** and **ZnP-B2**, Chart 1), or so-called $A_4$-porphyrins/benzoporphyrins, were used as efficient ternary components for bulk-heterojunction solar cells.[54] Another study from our group demonstrated possible solid-state polymerization of a bithiophene-containing benzoporphyrin derivative and formation of polaron in its polymeric system by using in-depth spectroscopic techniques.[55] Herein, we aim to study further the potential of the porphyrin- and benzoporphyrin-thiophene conjugates for the electrochemical reduction of $CO_2$. Additionally, we designed novel porphyrins (**ZnP-3** and **ZnP-4**, Chart 1) and benzoporphyrins (**ZnBP-3** and **ZnBP-4**, Chart 1) having two electropolymerizable thienyl or bithiophenyl units and two phenyl groups in a *trans*-$A_2B_2$ fashion. Introduction of 2−4 polymerizable units allowed porphyrin and benzoporphyrin macrocycles to embed into an oligothiophenyl network, which hypothetically should enhance the stability of films and provide electrochemical activities for the electrochemical reduction of $CO_2$. While the tetrasubstituted monomers can provide higher polymerization sites around the macrocycles, the *trans*-disubstituted ones can give well-ordered linear polymer films, which should have different morphologies and therefore electrocatalytic behaviors from those obtained from their tetrasubstituted analogs.

## 2. EXPERIMENTAL SECTION

**2.1. Materials and Methods.** All chemicals were of analytical grade, purchased from commercial sources, and used as received. $^1$H-nuclear magnetic resonance (NMR) (400 MHz) and $^{13}$C NMR (100 MHz) spectra were recorded in $CDCl_3$, $D_2O$, or $(CD_3)_2SO$. Chemical shifts ($\delta$) are reported in ppm relative to the residual $CHCl_3$ signal (7.26 and 77.0 ppm for the $^1$H NMR and $^{13}$C NMR spectroscopy, respectively), $H_2O$ signal ($\delta$ = 4.78 ppm for $^1$H NMR spectroscopy), and $(CH_3)_2SO$ signal (2.50 and 39.5 ppm for $^1$H NMR and $^{13}$C NMR spectroscopy, respectively). The mass spectra were obtained using high-resolution electrospray ionization mass spectrometry (HR-ESI-MS) and matrix-assisted laser desorption ionization-time-of-flight mass spectrometry (MALDI-TOF-MS) using dithranol as a matrix. Absorption spectra of the solutions were measured in toluene at room temperature by a UV−visible spectrophotometer, and molar extinction coefficients ($\varepsilon$) were reported in $L{\cdot}mol^{-1}{\cdot}cm^{-1}$. In addition, the absorption spectra of the films on indium tin oxide-coated glass (ITO/glass) substrates were investigated at room temperature by the UV−visible spectrophotometer. Monomer films were prepared by drop-casting 10 $mg{\cdot}mL^{-1}$ solutions of target compounds in tetrahydrofuran (THF) on the ITO/glasses. Emission spectra of the solutions were recorded in toluene at room temperature by using a luminescence spectrophotometer. X-ray data of **Zn−P3** were collected on a Bruker X8 diffractometer with an APEX II CCD detector. A structure was refined by full-matrix least-squares methods on $F^2$ with SHELXL-2018/3[56] using the GUI Olex2.[57] The phenyl rings are 1:1 and the thienyl rings are 66:34 disordered. Suitable restraints must be applied. Both methanol molecules coordinated to a $Zn^{II}$ center are half occupied, and the total occupancy of the methanol molecules coordinated to a metal center was therefore only one. As a consequence of this, the coordination geometry of the $Zn^{II}$ center was square pyramidal and not octahedral. Dihedral angles were calculated by using the program Platon.[58] The graphical output was produced by the program Mercury.[59] CCDC 1985130 contains the supplementary crystallographic data for this paper. These data are provided free of charge by the Cambridge Crystallographic Data Centre.

**2.2. Noncommercial Compounds.** Dipyrromethanes **5**[60] and **6**,[61] 5,10,15,20-tetra(thiophen-2-ylporphyrinatozinc (**ZnP-1**),[54] 5,10,15,20-tetra(2,2′-bithiophen-5-yl)-tetrabenzoporphyrinatozinc (**ZnP-2**),[54] 5,10,15,20-tetra-(thiophen-2-yl)tetrabenzoporphyrinatozinc (**ZnBP-1**),[54] and 5,10,15,20-tetra(2,2′-bithiophen-5-yl)-tetrabenzoporphyrinatozinc (**ZnBP-2**)[54] were prepared by the previously reported procedures.

**2.3. 5,15-Bis(phenyl)-10,20-bis(thiophen-2-yl)-porphyrin (P-3).** According to a previous method,[62] a solution of compound **5** (0.672 g, 3.00 mmol), 2-thiophene carboxaldehyde (0.280 mL, 3.00 mmol), and $NH_4Cl$ (1.6 g, 30


https://doi.org/10.1021/acs.energyfuels.4c01824
Energy Fuels 2024, 38, 16555−16569

mmol) in acetonitrile (300 mL) was reacted with $BF_3{\cdot}OEt_2$ (24 μL, 0.30 mmol) under the $N_2$ atmosphere at 0 °C for 4 h. After that, DDQ (0.681 g, 3.00 mmol) was added, and the reaction mixture was stirred at room temperature for an additional hour. To quench the reaction, triethylamine (0.5 mL) was added and the solution was filtered through a pad of silica eluted by $CH_2Cl_2$. The filtrate was collected and concentrated to dryness. The resulting crude product was redissolved with toluene (120 mL) and treated with DDQ (0.681 g, 3.00 mmol). After refluxing for an hour, the resulting mixture was passed through a pad of silica using $CH_2Cl_2$ as the eluent. After removal of the solvents, the crude product was purified by a silica column (hexanes:$CH_2Cl_2$ = 1:1), followed by washing with hexanes and methanol under ultrasonic agitation to afford 5,15-bis(phenyl)-10,20-bis(2-thienyl)-porphyrin (**P-3**) as a purple solid (0.168 g, 18%). $^1$H NMR ($CDCl_3$) $\delta$ − 2.72 (s, 2H), 7.48−7.54 (m, 2H), 7.73−7.83 (m, 6H), 7.84−7.89 (m, 2H), 7.91−7.95 (m, 2H), 8.18−8.25 (m, 4H), 8.84 (d, $J$ = 4.4 Hz, 4H), 9.05 (d, $J$ = 4.4 Hz, 4H). Due to the low solubility of **P-3**, a well-resolved $^{13}$C-spectrum could not be obtained. HR-ESI-MS $m/z$: $[M + H]^+$ calcd for $C_{40}H_{26}N_4S_2$, 627.1672; found, 627.1677; $\lambda_{abs}$ 422, 518, 553, 595, 650 nm; $\lambda_{em}$ ($\lambda_{ex}$ = 422 nm) 660, 723 nm.

**2.4. 5,15-Bis(phenyl)-10,20-bis(thiophen-2-yl)-porphyrinatozinc(II) (ZnP-3).** Following a standard method,[63] a solution of **P-3** (31 mg, 0.050 mmol) in $CHCl_3$ (20 mL) was reacted with a solution of $Zn(OAc)_2{\cdot}2H_2O$ (55 mg, 0.25 mmol) in methanol (3 mL) at room temperature for 12 h. The resulting reaction mixture was washed with a 10% aqueous $NaHCO_3$ solution (20 mL) and deionized (DI) water (20 mL), and then dried over anhydrous $MgSO_4$. After that, the crude product was purified by a silica column ($CH_2Cl_2$), followed by washing with hexanes and methanol under ultrasonic agitation to yield 5,15-bis(phenyl)-10,20-bis-(thiophen-2-yl)porphyrinatozinc(II) (**ZnP-3**) as a purple solid (30 mg, 87%). $^1$H NMR ($CDCl_3$) $\delta$ 7.50 (dd, $J$ = 5.2, 3.6 Hz, 2H), 7.72−7.80 (m, 6H), 7.84 (dd, $J$ = 5.2, 1.2 Hz, 2H), 7.92 (dd, $J$ = 3.6, 1.2 Hz, 2H), 8.19−8.23 (m, 4H), 8.94 (d, $J$ = 4.8 Hz, 4H), 9.16 (d, $J$ = 4.8 Hz, 4H); $^{13}$C NMR ($CDCl_3$) $\delta$ 112.7, 122.0, 126.0, 126.7, 127.5, 127.8, 132.1, 132.4, 133.6, 134.5, 142.8, 143.8, 150.7, 151.2; HR-ESI-MS $m/z$: $[M + H]^+$ calcd for $C_{40}H_{24}N_4S_2Zn$, 689.0807; found, 689.0802; $\lambda_{abs}$ ($\varepsilon$) 426 ($4.7 \times 10^5$), 554, 594 nm; $\lambda_{em}$ ($\lambda_{ex}$ = 426 nm) 607, 653 nm. Single crystals of **ZnP-3** were grown by the slow evaporation of a $CHCl_3$/methanol solution.

**2.5. 5,15-Bis(phenyl)-10,20-bis(2,2′-bithiophen-5-yl)-porphyrin (P-4).** Following a previously reported procedure,[62] a solution of compound **5** (0.667 g, 3.00 mmol), 2,2′-bithiophene-5-carboxaldehyde (0.583 g, 3.00 mmol), and $NH_4Cl$ (1.6 g, 30 mmol) in acetonitrile (300 mL) was reacted with $BF_3{\cdot}OEt_2$ (24 μL, 0.30 mmol) under a $N_2$ atmosphere at 0 °C for 4 h. After that, the reaction mixture was treated with 2,3-dichloro-5,6-dicyano-1,4-benzoquinone (DDQ, 0.681 g, 3.00 mmol) at room temperature for an additional 1 h. After quenching the reaction by treating with triethylamine (0.5 mL), the solution was passed through a pad of silica eluted with 2% THF in $CH_2Cl_2$. Then, the crude product was reoxidized by refluxing with DDQ (0.681 g, 3.00 mmol) in toluene (120 mL) for an hour. The resulting solution was passed through a pad of silica eluted with 2% THF in $CH_2Cl_2$. After that, the crude product was purified by column chromatography (silica, hexanes:$CH_2Cl_2$ = 1:1), followed by washing with hexanes and methanol under ultrasonic agitation to obtain 5,15-bis(phenyl)-10,20-bis(2,2′-bithiophen-5-yl)-porphyrin (**P-4**) as a purple solid (0.148 g, 12%). $^1$H NMR ($CDCl_3$) $\delta$ −2.67 (s, 2H), 7.14 (dd, $J$ = 5.2, 3.6 Hz, 2H), 7.35 (dd, $J$ = 5.2, 1.2 Hz, 2H), 7.43 (dd, $J$ = 3.6, 1.2 Hz, 2H), 7.59 (d, $J$ = 3.6 Hz, 2H), 7.73−7.85 (m, 8H), 8.18−8.26 (m, 4H), 8.86 (d, $J$ = 4.8 Hz, 4H), 9.19 (d, $J$ = 4.8 Hz, 4H). Due to the low solubility of **P-4**, a well-resolved $^{13}$C-spectrum could not be obtained. HR-ESI-MS $m/z$: $[M + H]^+$ calcd for $C_{48}H_{30}N_4S_4$, 791.1426; found, 791.1424; $\lambda_{abs}$ 429, 520, 561, 594, 656 nm; $\lambda_{em}$ ($\lambda_{ex}$ = 429 nm) 671, 730 nm.

**2.6. 5,15-Bis(phenyl)-10,20-bis(2,2′-bithiophen-5-yl)-porphyrinatozinc(II) (ZnP-4).** Following a standard metalation method,[63] a solution of **P-4** (79 mg, 0.10 mmol) in $CHCl_3$ (40 mL) was reacted with a solution of $Zn(OAc)_2{\cdot}2H_2O$ (0.110 g, 0.500 mmol) in methanol (5 mL) at room temperature for 12 h. After that, the reaction solution was washed with a 10% aqueous $NaHCO_3$ solution (40 mL), deionized (DI) water (40 mL), and then brine (40 mL). After drying over anhydrous $MgSO_4$, the mixture was concentrated to dryness and the resulting crude product was purified by a silica column (1% THF in $CH_2Cl_2$), followed by washing with hexanes and methanol to afford 5,15-bis(phenyl)-10,20-bis(2,2′-bithiophen-5-yl)porphyrinatozinc(II) (**ZnP-4**) as a purple solid (71 mg, 83%). $^1$H NMR ($(CD_3)_2SO$) $\delta$ 7.22 (dd, $J$ = 5.2, 3.6 Hz, 2H), 7.58 (dd, $J$ = 3.6, 1.2 Hz, 2H), 7.65 (dd, $J$ = 5.2, 1.2 Hz, 2H), 7.76 (d, $J$ = 3.6 Hz, 2H), 7.78−7.88 (m, 6H), 7.90 (d, $J$ = 3.6 Hz, 2H), 8.16−8.24 (m, 4H), 8.81 (d, $J$ = 4.8 Hz, 4H), 9.16 (d, $J$ = 4.8 Hz, 4H); $^{13}$C NMR ($(CD_3)_2SO$) $\delta$ 110.9, 121.3, 123.2, 124.3, 125.7, 126.6, 127.6, 128.5, 131.5, 132.0, 134.1, 134.3, 136.3, 138.8, 142.2, 142.4, 149.7, 150.0; HR-ESI-MS $m/z$: $[M+2H]^+$ calcd for $C_{48}H_{28}N_4S_4Zn$, 854.0645; found, 854.0637; $\lambda_{abs}$ ($\varepsilon$) 432 ($3.2 \times 10^5$), 550, 600 nm; $\lambda_{em}$ ($\lambda_{ex}$ = 432 nm) 625 nm.

**2.7. 5,15-Bis(phenyl)-10,20-bis(thiophen-2-yl)-tetrabenzoporphyrinatocopper(II) (CuBP-3).** Following a previously reported procedure,[64] a mixture of compound **6** (0.627 g, 1.32 mmol) and KOH (0.741 g, 13.2 mmol) in ethylene glycol (13 mL) was refluxed for 1 h. After that, the reaction mixture was cooled to room temperature and diluted with $CH_2Cl_2$ (25 mL). The resulting solution was washed with DI water (2 × 25 mL) and brine (25 mL), and then dried over anhydrous $Na_2SO_4$. After removal of the solvent, the crude solid was redissolved with $CH_2Cl_2$ (10 mL) and the solution was then passed through a short silica column using $CH_2Cl_2$ as an eluent. The pale brown fraction was collected and concentrated to dryness, affording a brown oil containing a corresponding decarboxylated product (0.417 g), which was immediately used in the next step without further purification. With a slight modification from a previous procedure,[65] a solution of this oil in $CH_2Cl_2$ (50 mL) was treated with 2-thiophene carboxaldehyde (0.130 mL, 1.39 mmol) and $BF_3{\cdot}OEt_2$ (0.016 mL, 0.126 mmol) under the $N_2$ atmosphere at 0 °C, and then the reaction was continued at room temperature for 12 h. After that, $p$-chloranil (0.310 g, 1.26 mmol) was added to the reaction mixture, and then the stirring was continued at room temperature for additional 6 h. Subsequently, the reaction mixture was filtered through a pad of silica eluted with EtOAc. After removal of the solvents, the crude product was further purified by column chromatography using gradient elution (silica, from $CH_2Cl_2$ to $CH_2Cl_2$:EtOAc = 1:1). The purple fraction was collected and concentrated to dryness, leading to a dark purple solid (0.191 g) that was dissolved in $CHCl_3$ (60 mL) and treated with a solution of


https://doi.org/10.1021/acs.energyfuels.4c01824
Energy Fuels 2024, 38, 16555−16569

$Cu(OAc)_2·H_2O$ (0.300 mg, 1.15 mmol) in methanol (7 mL) at room temperature.[63] After 12 h, the solution was washed with a 10% aqueous $NaHCO_3$ solution (60 mL), DI water (60 mL), and then brine (60 mL), and dried over anhydrous $MgSO_4$. After removal of the solvent, the resulting crude product was purified by column chromatography (silica, hexanes:$CH_2Cl_2$ = 1:1), followed by washing with hexanes and methanol under ultrasonic agitation, affording as a dark purple solid **Cu-7** (0.162 g). MALDI-TOF-MS *m/z* (%): found, 902.841 (100) [$M^+$]; calcd, 904.694 ($M^+$; M = $C_{56}H_{48}CuN_4S_2$). Due to the low solubility of this compound, other spectroscopic data could not be obtained properly. This solid was directly used in a further step.

Following a published procedure,[66] a solution of the resulting solid containing **Cu-7** (0.162 g) and DDQ (0.650 g, 2.86 mmol) in THF (100 mL) was refluxed for 60 min. After cooling down to room temperature, the solvent was removed under reduced pressure, and the resulting crude was redissolved with $CH_2Cl_2$ (100 mL). Then, the solution was washed with a 10% aqueous solution of $Na_2SO_3$ (100 mL) and brine (100 mL), dried over $MgSO_4$, and concentrated to dryness. The crude product was purified by a silica column ($CH_2Cl_2$), followed by washing with hexanes and methanol under ultrasonic agitation to afford **CuBP-3** as a dark green solid (62 mg, 8% from compound **6**). MALDI-TOF-MS *m/z* (%): found, 887.495 [$M^+$]; calcd, 888.566 ($M^+$, M = $C_{56}H_{32}CuN_4S_2$); $\lambda_{abs}$ 465, 605, 656 nm. Upon excitation at 465 nm, no emission peak was observed.

**2.8. 5,15-Bis(phenyl)-10,20-bis(thiophen-2-yl)-tetrabenzoporphyrin (BP-3).** A solution of **CuBP-3** (62 mg, 0.070 mmol) in $CH_2Cl_2$ (120 mL) was treated with conc. HCl (6.50 mL) dropwise at 0 °C. Then, the reaction mixture was stirred at room temperature for 90 min, and the solution was poured into DI water (120 mL). After that, the organic layer was collected, washed with a saturated $NaHCO_3$ solution (2 × 120 mL) and brine (120 mL), dried over anhydrous $MgSO_4$, and concentrated to dryness. The resulting crude product was purified by column chromatography (silica, hexanes:$CH_2Cl_2$ = 1:1), followed by washing with hexanes and methanol under ultrasonic agitation to obtain **BP-3** as a green solid (43 mg, 74%). $^1$H NMR ($CDCl_3$) $\delta$ −1.12 (s, 2H), 6.91−7.35 (m, 16H), 7.59−7.65 (m, 2H), 7.87 (t, *J* = 7.2 Hz, 4H), 7.90−7.98 (m, 4H), 7.99 (m, 2H), 8.36 (br s, 4H). Due to the low solubility of **BP-3**, a well-resolved $^{13}$C-spectrum could not be obtained. MALDI-TOF-MS *m/z* (%): found, 826.379 (100) [$M^+$]; calcd, 827.036 ($M^+$; *M* = $C_{56}H_{34}N_4S_2$), $\lambda_{abs}$ 468, 592, 631, 640, 703 nm; $\lambda_{em}$ ($\lambda_{ex}$ = 468 nm) 710, 792 nm.

**2.9. 5,15-Bis(phenyl)-10,20-bis(thiophen-2-yl)-tetrabenzoporphyrinatozinc(II) (ZnBP-3).** Following a standard procedure,[63] a solution of **BP-3** (43 mg, 0.052 mmol) in $CHCl_3$ (52 mL) was reacted with a solution of $Zn(OAc)_2·2H_2O$ (57 mg, 0.26 mmol) in methanol (6 mL) at room temperature for 15 min. After that, the reaction solution was washed with a 10% aqueous $NaHCO_3$ solution (50 mL), water (50 mL), and brine (50 mL), and dried over anhydrous $MgSO_4$. The solvent was removed under reduced pressure, and the crude product was purified by a silica column ($CH_2Cl_2$), followed by washing with hexanes and methanol under ultrasonic agitation to obtain **ZnBP-3** as a purple solid (44 mg, 96%). $^1$H NMR ($CDCl_3$) $\delta$ 7.15 (d, *J* = 8.4 Hz, 4H), 7.27−7.34 (m, 4H), 7.34−7.45 (m, 8H), 7.64 (dd, *J* = 5.2, 3.6 Hz, 2H), 7.87 (t, *J* = 7.6 Hz, 4H), 7.90−7.98 (m, 4H), 8.00 (dd, *J* = 5.2, 0.8 Hz, 2H), 8.29 (d, *J* = 7.2 Hz, 4H); $^{13}$C NMR ($CDCl_3$) $\delta$ 108.0, 118.0, 124.2, 124.6, 125.8, 125.9, 128.1, 128.7, 129.1, 129.2, 132.5, 134.3, 138.6, 138.7, 143.1, 143.8, 144.6, 146.0; HR-ESI-MS *m/z*: [$M$]$^+$ calcd for $C_{56}H_{32}N_4S_2Zn$, 888.1360; found, 888.1382; $\lambda_{abs}$ ($\varepsilon$) 463 ($3.0 \times 10^5$), 608, 660 ($8.1 \times 10^4$) nm; $\lambda_{em}$ ($\lambda_{ex}$ = 463 nm) 670, 732 nm.

**2.10. 5,15-Bis(phenyl)-10,20-bis(2,2′-bithiophen-5-yl) Tetrabenzoporphyrinatocopper(II) (CuBP-4).** In the similar manner as described for **CuBP-3**, dipyrromethane **6** (1.436 g, 3.02 mmol) was reacted with KOH (1.694 g, 30.2 mmol) in ethylene glycol (30 mL) under reflux for 1 h.[64] Then, the resulting brown oil (0.970 g) was dissolved in $CH_2Cl_2$ (120 mL) and then treated with 2,2′-bithiophene-5-carboxaldehyde (0.626 g, 3.22 mmol) and $BF_3·OEt_2$ (37 $\mu$L, 0.29 mmol), followed by oxidation with *p*-chloranil (1.081 g, 4.395 mmol).[65] After that, the resulting mixture was passed through a pad of silica eluted with a solution of 10% THF in $CH_2Cl_2$ and the filtrate was then concentrated to dryness. Subsequent column chromatography (silica, $CH_2Cl_2$:EtOAc = 1:1) led to a purplish black solid (0.481 g) that was dissolved in $CHCl_3$ (120 mL) and reacted with a solution of $Cu(OAc)_2·H_2O$ (0.479 g, 2.40 mmol) in methanol (15 mL) at room temperature for 12 h.[63] After a workup process, the resulting crude product was purified by a silica column (hexanes:$CH_2Cl_2$ = 1:3) and washed with hexanes and methanol under ultrasonic agitation, affording a dark purple solid containing **Cu-8** (0.311 g). MALDI-TOF-MS *m/z* (%): found, 1067.380 [$M^+$]; calcd, 1068.934 ($M^+$, *M* = $C_{64}H_{52}CuN_4S_4$). Due to the low solubility of this compound, other spectroscopic data could not be obtained. After that, this solid was reacted with DDQ (1.051 g, 4.63 mmol) in THF (200 mL) under reflux for 1 h.[66] After a workup process and then purification by column chromatography (silica, $CH_2Cl_2$), the resulting solid was washed with hexanes and methanol under ultrasonic agitation to give **CuBP-4** as a dark green solid (90 mg, 6% from compound **6**). MALDI-TOF-MS *m/z* (%): found, 1051.584 [$M^+$]; calcd, 1052.806 ($M^+$, *M* = $C_{64}H_{36}CuN_4S_4$); $\lambda_{abs}$ 461, 655 nm. Upon excitation at 461 nm, no significant emission peak was observed.

**2.11. 5,15-Bis(phenyl)-10,20-bis(2,2′-bithiophen-5-yl) Tetrabenzoporphyrin (BP-4).** Following the demetalation procedure described for **BP-4**, a solution of **CuBP-4** (99 mg, 0.094 mmol) in $CH_2Cl_2$ (150 mL) was reacted with conc. HCl (10 mL) at 0 °C and the reaction mixture was stirred at room temperature for 1 h. After a workup process, purification by a silica column (hexanes:$CH_2Cl_2$ = 1:1), and then washing with methanol under ultrasonic agitation, **BP-4** was yielded as a green solid (62 mg, 67%).[1] H NMR ($CDCl_3$) −1.09 (s, 2H), 6.98−7.19 (m, 4H), 7.14−7.19 (m, 2H), 7.28−7.83 (m, 12H), 7.38 (d, *J* = 4.8 Hz, 2H), 7.48 (d, *J* = 3.2 Hz, 2H), 7.71 (d, *J* = 3.2 Hz, 2H), 7.83−7.91 (m, 6H), 7.91−7.98 (m, 2H), 8.37 (br s, 4H). Due to the low solubility of **BP-4**, a well-resolved $^{13}$C-spectrum could not be obtained. MALDI-TOF-MS *m/z* (%): found, 990.903 [$M^+$]; calcd, 991.276 ($M^+$, *M* = $C_{60}H_{38}N_4S_4$), $\lambda_{abs}$ 476, 594, 633, 644, 705 nm; $\lambda_{em}$ ($\lambda_{ex}$ = 476 nm) 713, 795 nm.

**2.12. 5,15-Bis(phenyl)-10,20-bis(2,2′-bithiophen-5-yl) Tetrabenzoporphyrinatozinc(II) (ZnBP-4).** Following a standard metalation procedure[63] and the method described for **ZnBP-3**, a solution of **BP-4** (24 mg, 0.024 mmol) in $CHCl_3$ (25 mL) was treated with a solution of $Zn(OAc)_2·2H_2O$ (26 mg, 0.12 mmol) in methanol (3 mL) at room temperature for 15 min. After a workup step and purification


https://doi.org/10.1021/acs.energyfuels.4c01824
Energy Fuels 2024, 38, 16555−16569

Table 1. Electrochemical Behavior of the Target Porphyrins and Benzoporphyrins and their Homogeneous Electrocatalytic Activities Toward the Electrochemical Reduction of $CO_2$

| | | $E_{peak,red}/V$ ($J_{peak}/\mu A \cdot cm^{-2}$) | | | headspace product analysis | | |
|---|---|---|---|---|---|---|---|
| compound | condition | first reduction | second reduction | third reduction | applied potential/V | CO/$\mu$mol | % FE |
| Porphyrins | | | | | | | |
| **ZnP-1** | $N_2$ | −1.03 (47) | −1.46 (68) | −1.59 (70) | −1.37 | 0.10 | 2 |
| | $CO_2$ | −1.03 (58) | −1.43 (148) | −1.58 (159) | | | |
| **ZnP-2** | $N_2$ | −0.95 (64) | −1.36 (85) | −1.47 (90) | −1.27 | 0.14 | 1 |
| | $CO_2$ | −0.95 (63) | −1.34 (138) | −1.48 (187) | | | |
| **ZnP-3** | $N_2$ | −1.07 (25) | −1.50 (35) | N.A.[a] | −1.42 | 0.22 | 2 |
| | $CO_2$ | −1.06 (27) | −1.49 (68) | N.A.[a] | | | |
| **ZnP-4** | $N_2$ | −1.05 (36) | −1.47 (54) | N.A.[a] | −1.42 | N.A.[b] | N.A.[b] |
| | $CO_2$ | −1.04 (46) | −1.43 (78) | N.A.[a] | | | |
| Benzoporphyrins | | | | | | | |
| **ZnBP-1** | $N_2$ | −1.07 (64) | −1.40 (97) | N.A.[a] | −1.57 | 1.43 | 9 |
| | $CO_2$ | −1.06 (65) | −1.38 (98) | N.A.[a] | | | |
| **ZnBP-2** | $N_2$ | −0.99 (46) | −1.30 (62) | −1.61 (94) | −1.57 | 0.41 | 2 |
| | $CO_2$ | −0.96 (43) | −1.25 (66) | −1.56 (198) | | | |
| **ZnBP-3** | $N_2$ | −1.13 (72) | −1.46 (103) | N.A.[a] | −1.62 | 0.92 | 9 |
| | $CO_2$ | −1.12 (72) | −1.44 (112) | N.A.[a] | | | |
| ZnBP-4 | $N_2$ | −1.09 (48) | −1.39 (70) | N.A.[a] | −1.62 | 0.74 | 8 |
| | $CO_2$ | −1.07 (50) | −1.37 (68) | N.A.[a] | | | |

[a]No peak was observed. [b]No product was detected.

by a silica column ($CH_2Cl_2$), followed by washing with hexanes and methanol under ultrasonic agitation, **ZnBP-4** was obtained as a bluish green solid (24 mg, 94%). $^1$H NMR ($CDCl_3$) $\delta$ 7.12−7.20 (m, 6H), 7.28−7.34 (m, 4H), 7.36−7.39 (m, 2H), 7.39−7.45 (m, 4H), 7.45−7.49 (m, 2H), 7.73 (d, $J$ = 3.6 Hz, 2H), 7.78 (d, $J$ = 8.0 Hz, 4H), 7.83 (d, $J$ = 3.6 Hz, 2H), 7.84−7.91 (m, 4H), 7.92−7.98 (m, 2H), 8.30 (br s, 4H); $^{13}$C NMR ($CDCl_3$) $\delta$ 107.6, 118.1, 124.4, 124.4, 124.6, 124.8, 126.0, 126.1, 128.2, 129.1, 129.2, 133.4, 134.3, 137.9, 138.4, 138.7, 140.8, 143.0, 143.9, 144.6, 144.7; HR-ESI-MS $m/z$: $[M]^+$ calcd for $C_{64}H_{36}N_4S_4Zn$, 1054.1100; found, 1054.1124; $\lambda_{abs}$ ($\varepsilon$) 470 ($2.3 \times 10^5$), 615, 663 ($6.3 \times 10^4$) nm; $\lambda_{em}$ ($\lambda_{ex}$ = 470 nm) 674, 739 nm.

**2.13. Homogeneous Electrocatalytic Activity Toward Electrochemical Reduction of $CO_2$.** All experiments were performed in a one-compartment three-electrode system consisting of a glassy carbon working electrode (WE), a AgCl-coated Ag wire (Ag/AgCl) quasi reference electrode (QRE), and a Pt plate counter electrode (CE). The Ag/AgCl QRE was prepared using a previously reported procedure[67] and externally calibrated with a ferrocene/ferrocenium couple of which a potential value of 0.72 V vs NHE in dimethylformamide (DMF) was used, resulting in a potential at 0.0 V vs Ag/Ag QRE of 0.33 V vs NHE.[68] The potentials presented in this work were referred to NHE. Cyclic voltammograms were recorded in a 0.1 M tetrabutylammonium hexafluorophosphate ($TBAPF_6$) electrolyte solution containing 0.5 mM of porphyrins or benzoporphyrins at a potential range between 0.33 V and −1.67 V vs NHE with a scan rate of 0.05 $V \cdot s^{-1}$ at room temperature under the $N_2$- and $CO_2$-saturated atmosphere. The solutions were purged with $N_2$ or $CO_2$ for 20 min prior to the measurements. Chronoamperometry (CA) or constant potential electrolysis (CPE) was performed at certain potentials as reported in Table 1 under a $CO_2$-saturated atmosphere for 20 h. Product analysis was performed by injecting 2 mL of headspace gas (total volume was 10 mL) from a reaction vial into Thermo Scientific TraceUltra gas chromatography (GC) equipped with a thermal conductivity detector (TCD). The peak area of CO formation collected from each experiment was used to determine the quantity of CO in the headspace gas using a premeasured calibration curve. The NMR spectroscopy was used to investigate the products in liquid phases in $D_2O$ and DMSO-$d_6$. The results indicated that there was no carbon-based reduction product in any samples.

**2.14. Electropolymerization of Bithiophenyl-Substituted Derivatives.** Following a previous study,[69] the electropolymerization of **ZnP-2**, **ZnP-4**, and **ZnBP-2** was performed in the one-compartment three-electrode system by means of cyclic voltammetry (CV) in a $CH_2Cl_2$ solution containing 0.1 M $TBAPF_6$ and the 0.2 mM monomer. The ITO/glass was used as the WE and as the substrate for the newly formed polymer, and the Pt plate and Ag/AgCl were used as the CE and QRE, respectively. The polymerization was carried out potentiodynamically under the $N_2$ atmosphere at the potentials ranging from 0.33 to 1.93 V for **ZnP-2** and **ZnP-4**, and from 0.33 to 1.83 V for **ZnBP-2** at the scan rate of 0.05 $V \cdot s^{-1}$ for 10 cycles. In the case of **ZnBP-4**, the electropolymerization was performed in the similar manner in a 0.1 M $TBAPF_6$ electrolyte solution in DMF at the potentials ranging from 0.33 to 2.08 V when the ITO/glass was used as the substrate, or from 0.33 to 1.83 V when a carbon paper was employed. The thickness and roughness of the resulting films on the ITO/glasses were measured by a Dektak XTL Profilometer and Bruker Innova AFM, respectively.

**2.15. Heterogeneous Catalytic Activity Toward Electrochemical Reduction of $CO_2$.** All experiments were conducted in a one-compartment, three-electrode electrochemical cell containing 0.1 M $TBAPF_6$ in acetonitrile as the electrolyte solution. The carbon paper coated with **p-ZnBP-4** was used as the WE, and the Pt plate and Ag/AgCl were used as the CE and the QRE, respectively. The cyclic voltammograms were recorded at the potential between 0.33 V and −1.57 V at the scan rate of 0.05 $V \cdot s^{-1}$ for 3 cycles under the $N_2$ and $CO_2$ atmosphere. The CPE was subsequently performed at −1.57 V under a $CO_2$ atmosphere for 3 h. Headspace product


https://doi.org/10.1021/acs.energyfuels.4c01824
Energy Fuels 2024, 38, 16555−16569

analysis was carried out in the similar manner as described for the homogeneous experiments. The NMR spectroscopy was also used to investigate the products in liquid phases and detected no carbon-based reduction product in any samples.

**2.16. Calculation Details.** All calculations were carried out using the Gaussian 16 software package.[70] Density functional theory (DFT) calculations were performed using the B3LYP functional[71,72] with the 6-311G(d,p) basis set, including dispersion effects to determine accurate interaction energies. Dispersion effects were found using the D3 Grimme's dispersion correction[73] with Becke−Johnson damping (GD3BJ).[74] Frequency calculations were performed to take Gibbs free energy corrections into account for ambient conditions (298.15 K and 1 atm).

## 3. RESULTS AND DISCUSSION

**3.1. Synthesis and Characterization.** Synthesis of the target *trans*-$A_2B_2$-porphyrins started from acid-catalyzed condensation of dipyrromethane **5**[60] and a corresponding aldehyde in acetonitrile in the presence of $BF_3{\cdot}OEt_2$ and $NH_4Cl$ at 0 °C for 4 h, followed by oxidation with DDQ,[62] affording freebase porphyrins **P-3** and **P-4** in 12−18% (Scheme 1).

Formation of **P-3** and **P-4** was confirmed by HR-ESI-MS, exhibiting their molecular ion peaks at $m/z$ 627.1677 and 791.1424, respectively. Subsequent zinc metalation of **P-3** and **P-4** under a known procedure[63] quantitatively yielded **ZnP-3** and **ZnP-4**, respectively, whose formation was confirmed by their HR-ESI mass spectra exhibiting the molecular ion peaks at $m/z$ 689.0802 and 854.0645, respectively. The complete metalation of the freebase precursors was proven by disappearance of the peaks of inner protons of the macrocycles at around −2.70 ppm (ppm) in their $^1$H NMR spectra and the emission peaks at 723−730 nm, which were observed for **P-3** and **P-4**.

**Scheme 1. Synthesis of *trans*-$A_2B_2$-Porphyrins ZnP-3 and ZnP-4**

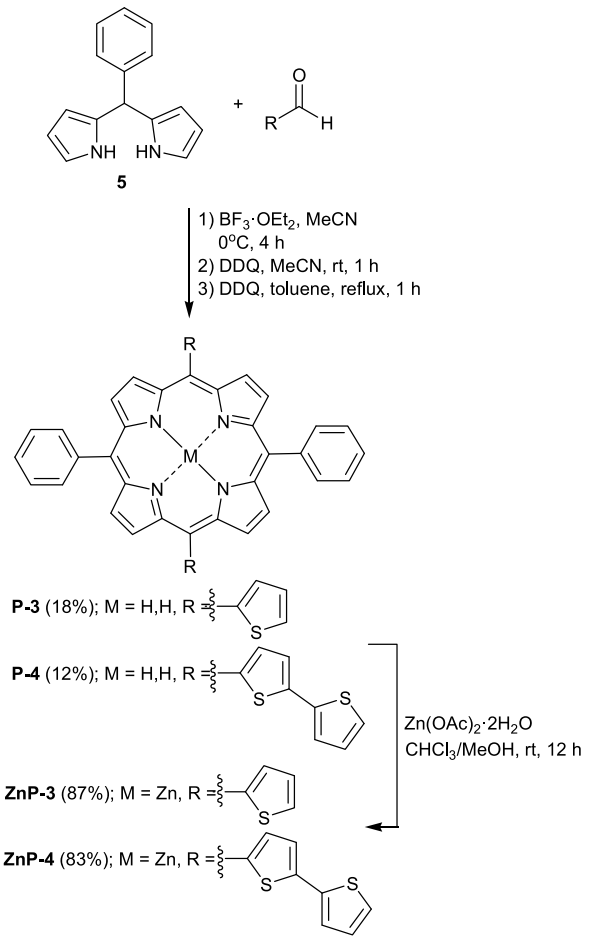


As regards the synthesis of **ZnBP-3** and **ZnBP-4**, we observed that the corresponding freebase benzoporphyrins could not be easily prepared due to low stability of their tetracyclohexanoporphyrin precursors under common oxidation condition using *p*-chloranil or DDQ. This is attributed to rapid formation of unstable dication intermediates as described in a previous report.[66] Therefore, a template-directed approach by using $Cu(OAc)_2{\cdot}H_2O$ was employed, leading to efficient construction of Cu(II)-porphyrins **Cu-7** and **Cu-8** that could tolerate the aromatization condition and readily demetalate to form desirable freebase benzoporphyrins **BP-3** and **BP-4** (Scheme 2).[66] Preparation of porphyrin precursors **Cu-7** and **Cu-8** was carried via a four-step procedure starting from decarboxylation of compound **6**,[64] condensation of the resulting dipyrromethane with an appropriate aldehyde in the presence of $BF_3{\cdot}OEt_2$,[65] oxidation with *p*-chloranil,[66] and then Cu-metalation of the resulting porphyrin.[63] The MALDI-TOF-MS confirmed the formation of **Cu-7** and **Cu-8** by showing their molecular ion peaks at $m/z$ 902.841 and 1068.934, respectively. Due to the low solubility of these compounds, the aromatization step was performed in a refluxing solution of DDQ in THF for an hour without chromatographic purification, affording **CuBP-3** and **CuBP-4** in 8% and 6%, respectively, overall yields from compound **6**. Based on thin-layer chromarography (TLC) and MALDI-TOF-MS, the low yield is attributed to competitive oligomerization of dipyrromethane and decomposition under the refluxing DDQ-aromatization condition. MALDI-TOF mass spectra of **CuBP-3** and **CuBP-4** showed their molecular ion peaks at $m/z$ 887.495 and 1051.112, respectively.

The demetalation of **CuBP-3** and **CuBP-4** was achieved by a reaction with concentrated HCl in $CH_2Cl_2$ at room temperature for 60−90 min, leading to **BP-3** and **BP-4** in 74% and 67%, respectively. Instead of using $H_2SO_4$ as reported in a previous procedure,[66] the concentrated HCl was chosen in this case to prevent unwanted sulfonation of thiophene units.[75] Formation of **BP-3** and **BP-4** was confirmed by their molecular ion peaks in the MALDI-TOF mass spectra at $m/z$ 826.379 and 990.903, respectively. To obtain the desirable Zn complexes, **BP-3** and **BP-4** were zinc-metalated with $Zn(OAc)_2{\cdot}2H_2O$ in $CHCl_3$/MeOH at room temperature for 15 min, affording **ZnBP-3** and **ZnBP-4** in 96% and 94%, respectively. Completion of the metalation step was confirmed by the disappearance of the emission peaks at 792−795 nm and the inner proton signals in their $^1$H NMR spectra observed in their freebase precursors. Additionally, the HR-ESI mass spectra exhibited the molecular ion peaks at $m/z$ 888.1382 and 1054.1124 for **ZnBP-3** and **ZnBP-4**, respectively.

**3.2. Photophysical Properties.** The absorption spectra of all porphyrins and benzoporphyrins exhibited characteristic peaks including intense Soret bands in a range of 400−500 nm and Q-bands at 500−700 nm (Figure 1). Absorption maxima ($\lambda_{abs,max}$) of the benzoporphyrin derivatives were red-shifted by 37−39 nm, compared with those of the porphyrin analogs


https://doi.org/10.1021/acs.energyfuels.4c01824
Energy Fuels 2024, 38, 16555−16569

**Scheme 2. Synthesis of *trans*-$A_2B_2$-Benzoporphyrins ZnBP-3 and ZnBP-4**

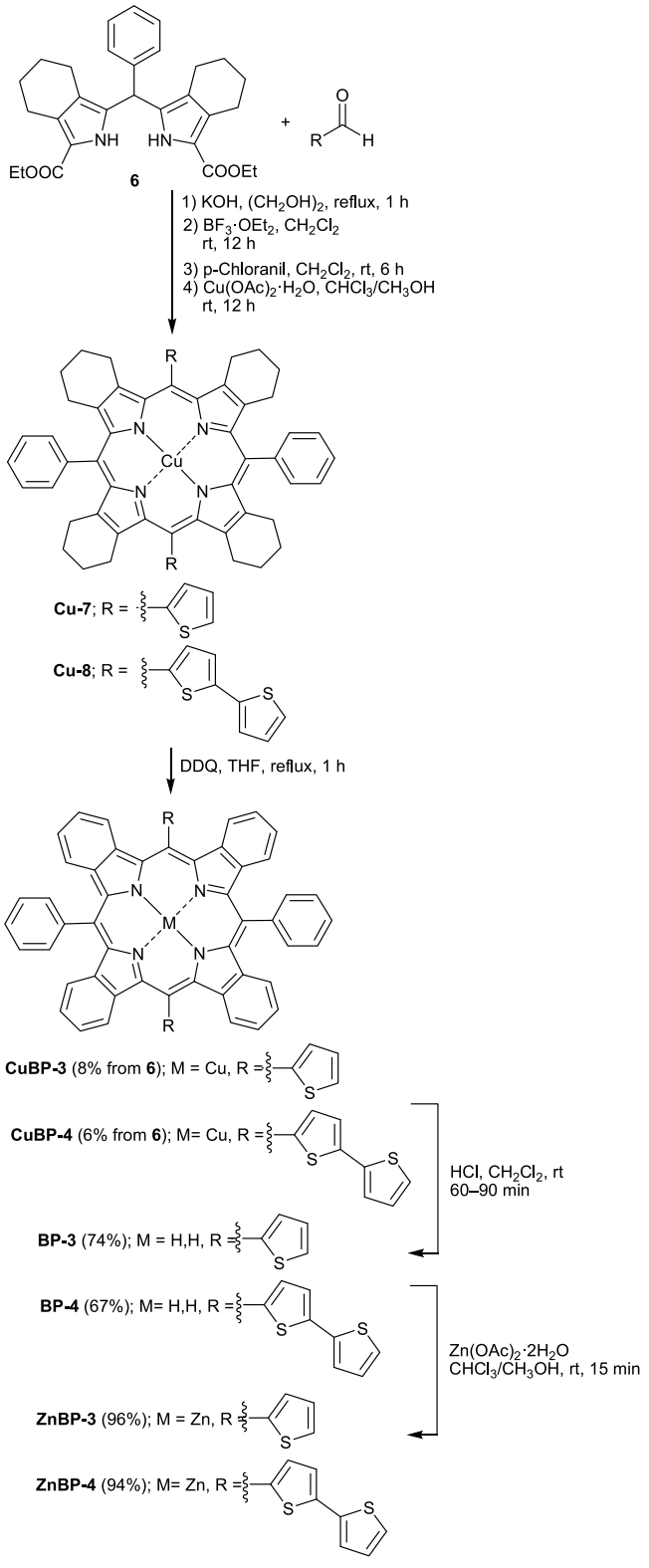


bearing the same *meso*-substitution patterns. This observation resulted from the extension of a $\pi$-conjugation system due to $\beta$-benzo fused rings on the porphyrin core. The impact of replacement of the phenyl *meso*-groups with the thienyl units on the macrocycle could be determined by comparing $\lambda_{abs,max}$ of **ZnP-3** and **ZnBP-3** with those of **ZnP-1** and **ZnBP-1** previously studied by our group, i.e., 436 and 476 nm, respectively.[54] The result revealed that $\lambda_{abs,max}$ of **ZnP-1** and **ZnBP-1** was red-shifted by 10−13 nm, indicating more efficient electronic communication between the macrocycles and the *meso*-substituents when the thienyl groups were present. This red shift was stronger, namely, by 17−18 nm when comparing $\lambda_{abs,max}$ of **ZnP-4** and **ZnBP-4** with those of **ZnP-2** and **ZnBP-2**, formerly reported at 450 and 487 nm,[54] respectively. Additionally, the introduction of the additional thiophene rings on the $\alpha$-positions of the thienyl groups of **ZnP-3** and **ZnBP-3** caused the red shift of $\lambda_{abs,max}$ by 6−7 nm as observed for **ZnP-4** and **ZnBP-4**.

Figure 1 also demonstrated that the $\beta$-benzo fused rings on the porphyrin core, the additional thiophene rings on the $\alpha$-positions of the thienyl groups, and the replacement of the phenyl *meso*-groups with the thienyl units on the macrocycle affected emission behavior of the molecules in a similar manner as observed in the cases of the absorption properties. Upon the excitation at $\lambda_{abs,max}$, emission maxima ($\lambda_{em,max}$) of the benzoporphyrins were red-shifted by 49−63 nm, compared with those of porphyrins bearing the same *meso*-substitution. The thienyl-substituted derivatives gave the red shift of 11−12 nm, compared with the phenyl-substituted ones, and the introduction of the additional thiophene rings on the $\alpha$-positions of the thienyl *meso*-groups caused further 4−18 nm red shift of the emission maxima.

The above-mentioned absorption and emission behavior was in good agreement with that observed in our previous work.[54] However, to provide a well-defined proof in addition to the prior data[54,76] for the impact of the thienyl *meso*-group on the electronic communication with the porphyrin macrocycle in comparison with the phenyl units, a crystal structure of **ZnP-3** was investigated by X-ray diffraction (XRD) analysis with a support from theoretical calculation data investigated by a Gaussian 16 program package at a B3LYP/6-311g(d,p) + GD3BJ level. As shown in Figure 2, the $Zn^{II}$ center of **ZnP-3** was found to be weakly bound to one methanol molecule (Zn−O = 2.418(6) Å). The dihedral angles between two planes of the disordered phenyl *meso*-substituents and that of the porphyrin macrocycle were found to be 70.4(5)° and 74.2(6)°, respectively. These values are consistent with those reported for a toluene solvate of tetraphenylporphinatozinc(II) (68.0° and 71.7°).[77] The dihedral angles between the two disordered thienyl rings and a porphyrin plane were found to be 68.3(5)° and 82.6(7)°, respectively.

Results from the DFT calculation were found to be more straightforward and corresponded to those from the XRD analysis, as shown in Figure 3. The dihedral angles between the two planes of the phenyl meso-substituents and that of the porphyrin macrocycle were determined to be 70.17°, while that between the two thienyl rings and the porphyrin plane were determined to be 79.19°. The data suggested that the thienyl rings were more twisted from the macrocycle plane, compared with the phenyl ones, because of steric hindrance.

To understand an electronic structure at the ground state (S0) of **ZnP-3**, its electrostatic potential (ESP) map was investigated. As shown in Figure 4, charges of thienyl group regions were more positive (blue color) than those of phenyl groups, indicating stronger intramolecular charge transfer from the thienyl substituents to the porphyrin macrocycle than that from the phenyl groups.

In addition, the electron density difference between the ground (S0) and excited states (S1) in the **ZnP-3** structure


https://doi.org/10.1021/acs.energyfuels.4c01824
Energy Fuels 2024, 38, 16555−16569

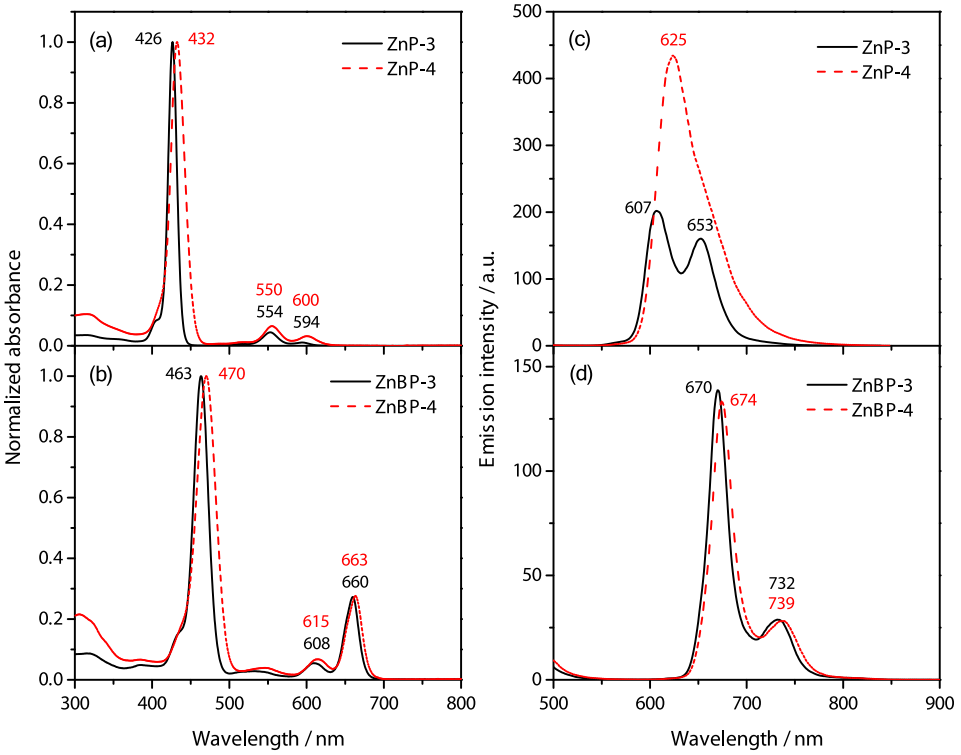


**Figure 1.** Normalized absorption spectra (black solid lines) of (a) *trans*-$A_2B_2$-porphyrins and (b) *trans*-$A_2B_2$-benzoporphyrins, and the emission spectra (red dashed lines) of (c) *trans*-$A_2B_2$-porphyrins and (d) *trans*-$A_2B_2$-benzoporphyrins.

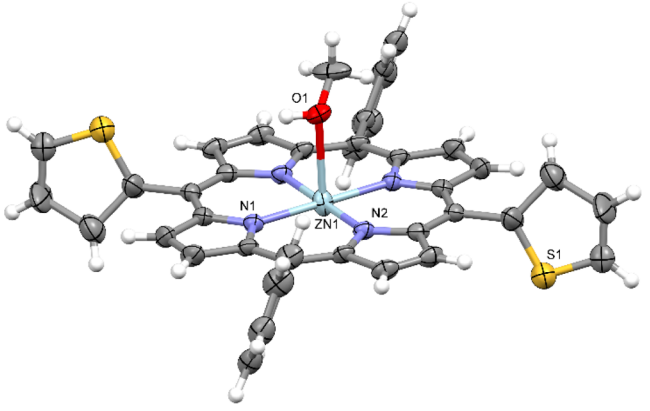


**Figure 2.** Crystal structure of ZnP-3 coordinated with one methanol molecule, showing 30% probability displacement ellipsoids and atom-numbering of selected atoms. The hydrogen atoms, minor components of the disordered phenyl and thienyl rings, and the second disordered methanol molecule are omitted for clarity.

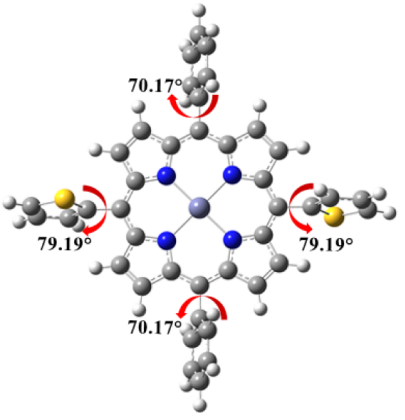


**Figure 3.** Structure and related dihedral angles of the ZnP-3 molecule analyzed by the Gaussian 16 program package at the B3LYP/6-311g(d,p) + GD3BJ level.

was studied to understand the electronic communication between those states. In Figure 5, a charge accumulation region is rendered in azure, whereas a charge depletion region is rendered in purple. The calculation showed that there was efficient electronic communication between the porphyrin macrocycle and the *meso*-thienyl rings as both colors were seen in these moieties. However, the depletion region was mainly located in the phenyl rings, indicating less electronic communication between the macrocycle and the phenyl *meso*-substituents, compared with the thienyl one. This result corresponded to the observation mentioned above and previously reported in our study on a series of tetrathienyl- and tetra(bithiophenyl)-substituted porphyrins.[54]

**3.3. Electrochemical Property and Preliminary Study on Homogeneous Electrochemical Reduction of $CO_2$.** In this study, CV was used to investigate the structure−electrochemical property relationship and electrocatalytic activity of the target porphyrins and benzoporphyrins toward the electrochemical reduction of $CO_2$. The electrochemical experiments of all compounds were performed in the one-compartment three-electrode system having the glassy carbon WE, the Ag/AgCl QRE, and the Pt CE. The cyclic voltammograms of 0.5 mM target compounds were recorded in DMF containing 0.1 M $TBAPF_6$ in the potential range between 0.33 V and −1.67 V, which was an electrochemical window determined from a control experiment under the $N_2$ and $CO_2$ atmosphere in the absence of the target compounds (Figure S51). Measurements were performed under $N_2$- and


https://doi.org/10.1021/acs.energyfuels.4c01824
Energy Fuels 2024, 38, 16555−16569

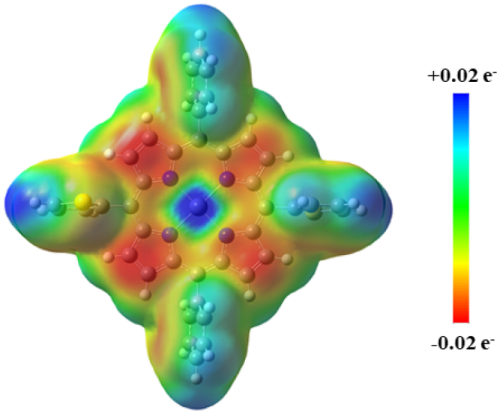


**Figure 4.** ESP map of a ZnP-3 molecule calculated using the Gaussian 16 program package at the B3LYP/6-311g(d,p) + GD3BJ level.

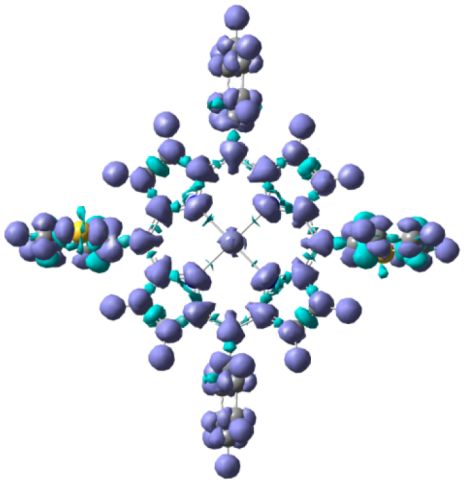

**Figure 5.** Electron density difference between S0 and S1 of the ZnP-3 molecule calculated using the Gaussian 16 program package at the B3LYP/6-311g(d,p) + GD3BJ level. The charge accumulation and depletion regions are colored azure and purple, respectively.

$CO_2$-saturated conditions for each compound in order to investigate its electrochemical behavior and electrocatalytic activity toward the electrochemical reduction of $CO_2$, respectively. The cyclic voltammograms of all eight compounds are shown in Figure 6, and reduction peak potentials ($E_{peak,red}$) and peak current density ($J_{peak}$) of each reduction step under the $N_2$- and $CO_2$-saturated conditions are summarized in Table 1.

Under $N_2$ saturation, the $A_4$-porphyrins **ZnP-1** and **ZnP-2** gave three semireversible reduction peaks at around −1.00, −1.50, and −1.60 V, which resulted from the reduction processes of the macrocylic ligand. This observation was consistent with the previous report on 5,10,15,20-tetraphenylporphyrinatozinc(II).[78] The effect of the extension of the $\pi$-conjugation system through the $\beta$-positions could be analyzed by comparing the reduction potentials of the semireversible ligand-centered reduction peaks of benzoporphyrins **ZnBP-1** and **ZnBP-2** with those of the corresponding porphyrins.[79] The results showed that the first and second reduction processes of the benzoporphyrin series occurred at 0.04−0.06 V more negative and 0.04−0.08 V more positive potential than their porphyrin analogs. Such shifts were also observed with the first two reduction peaks of benzoporphyrins **ZnBP-3** and **ZnBP-4** in comparison with porphyrins **ZnP-3** and **ZnP-4**, respectively. The third reduction peak was found only in **ZnBP-2** with the negative shift by 0.14 V, compared to **ZnP-2**. It was likely that the third reduction processes of **ZnBP-1**, **ZnBP-3**, and **ZnBP-4** occurred beyond the potential range of this study because of the effects explained hereafter. The replacement of the thienyl and bithiophenyl substituents in the $A_4$-porphyrin (derivatives **1** and **2**) with the phenyl groups on the macrocycles in the *trans*-$A_2B_2$-porphyrin (derivatives **3** and **4**) affected the $E_{peak}$ of the first and second reduction peaks to be more negative by 0.04−0.06 V and 0.09−0.11 V, respectively. This could explain why the third reduction peaks of **ZnP-3** and **ZnP-4** were also absent in this potential range, compared to **ZnP-1** and **ZnP-2**, respectively. The comparison between the thienyl and the bithiophenyl *meso*-substituted series, i.e., derivatives **1** vs **2** and derivatives **3** vs **4**, showed that the addition of another thiophene ring to thienyl *meso*-groups resulted in the positive shift of all reduction peaks by 0.02−0.12 V. This effect was more pronounced in the $A_4$-porphyrin (derivatives **1** vs **2**) and a reason for the missing third reduction peak of **ZnBP-1** in the potential range of the measurement.

Under the $CO_2$-saturated condition, the cyclic voltammograms of the porphyrin series showed the similar $E_{peak,red}$ as those recorded under the $N_2$ saturation with a slightly positive shift in some cases. Enhancement in $J_{peak}$ of 24−97 $\mu A \cdot cm^{-2}$ was observed in their second reduction steps, suggesting the possible electrocatalytic activity toward the reduction of $CO_2$. As regards the benzoporphyrin series, the CV showed that compared with the cyclic voltammograms recorded in the $N_2$-saturated solution, the electrochemical features observed at the first reduction step were almost identical, but the slight positive shift of $E_{peak}$ by 0.02−0.05 V was detected in the second reduction. The considerable increase in $J_{peak}$ was revealed at the potential beyond the second reduction steps as clearly seen in the third reduction of **ZnBP-2**, i.e., by 104 $\mu A \cdot cm^{-2}$. The positive shift of onset potentials and the sign of the current enhancement in the third reduction steps of **ZnBP-1**, **ZnBP-3**, and **ZnBP-4** could be seen, as well. However, since the experiments could not continue beyond the electrochemical window, the obvious increase in $J_{peak}$ of the third reduction step could not be recorded for these 3 compounds. The positive potential shift and the current enhancement suggested that the electrochemical $CO_2$ reduction should be mediated in the presence of benzoporphyrins as homogeneous catalysts.

To preliminarily investigate the catalytic performance of all compounds toward the electrochemical reduction of $CO_2$, the CPE was performed by applying a constant potential as presented in Table 1 for 20 h. The onset potentials of the second and third reduction peaks, where the current enhancement began to be pronounced, were used as the applied potentials for the CA of the porphyrin and benzoporphyrin series, respectively. According to the GC analysis of the headspace gas samples, the results revealed that CO was the only product observed from the electrochemical reduction of $CO_2$. Faradaic efficiency (FE) calculated based on the amount of CO production was found to be in the range of 1−2% for the porphyrins and 2−9% for the benzoporphyrins (Table 1). The higher efficiencies observed in the case of the benzoporphyrins probably resulted from the extended $\pi$-conjugation system at the $\beta$-positions of the macrocycle that might efficiently stabilize electrochemically active species generated during the electrochemical reduction of $CO_2$. As


https://doi.org/10.1021/acs.energyfuels.4c01824
Energy Fuels 2024, 38, 16555−16569

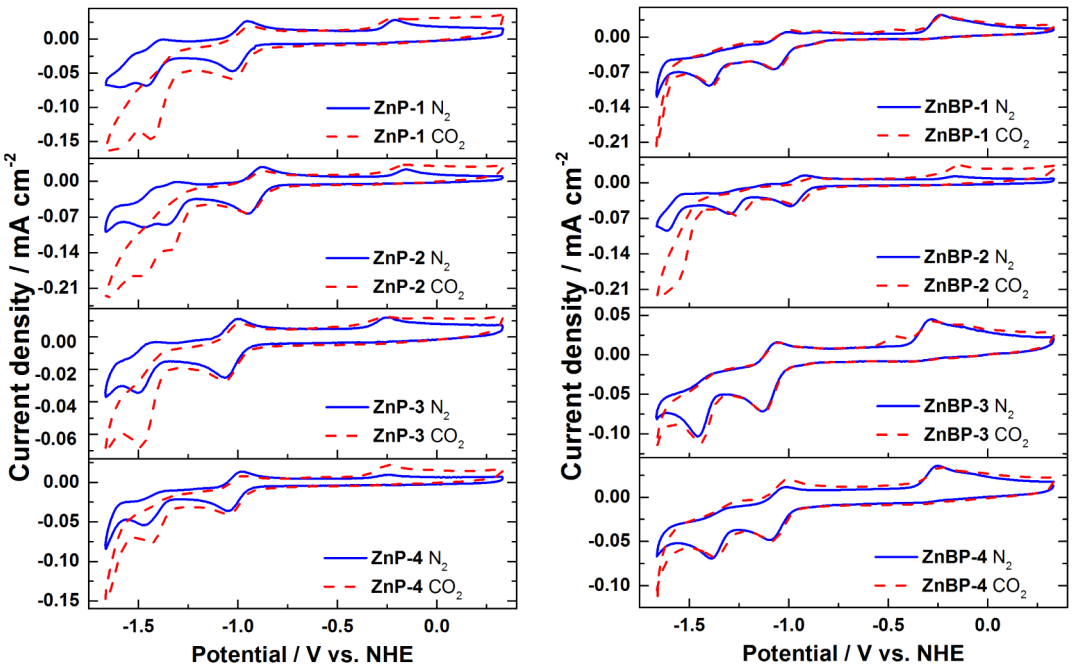


**Figure 6.** Cyclic voltammograms of the target porphyrins and benzoporphyrins under the $N_2$- and $CO_2$-saturated conditions (blue solid and red dashed lines, respectively).

**Table 2. Electrochemical Data from Electropolymerization and Morphology of the Resulting Polymer**

| | | $E_{peak,ox}$ relating to each molecular unit/V vs NHE | | | | | |
|---|---|---|---|---|---|---|---|
| compound | substrate | $\beta$-benzo fused ring | phenyl ring | macro-cycle | bithio-phenyl unit | film thickness/nm | film roughness/nm |
| **ZnP-2** | ITO/glass | -[a] | -[a] | 1.22 | 1.70 | 54 | 5.3 |
| **ZnP-4** | ITO/glass | -[a] | 1.19 | 1.34 | 1.84 | 58 | 2.8 |
| **ZnBP-2** | ITO/glass | 0.82 | -[a] | 1.05 | 1.60 | 115 | 12.4 |
| **ZnBP-4** | ITO/glass | 0.77 | -[b] | 1.01 | 1.72 | -[c] | -[c] |
| ZnBP-4 | carbon paper | 0.63 | -[b] | 1.08 | 1.57 | -[c] | -[c] |

[a]Compound has no such group. [b]Peak could not be clearly observed. [c]Value could not be determined due to very low film thickness on the ITO/glass or the high porosity of the carbon paper.

the control experiment, 20 h of electrolysis using the bare glassy carbon electrode was performed under the same conditions and no CO production was detected. It is noteworthy that an effort to add up to 3% v/v water into the electrolyte solution to further promote the above-mentioned proton-coupled pathway (eq 2) failed to give significant improvement in terms of CO productivity and other possible product formation.

**3.4. Electropolymerization of Bithiophenyl-Substituted Derivatives.** Following our previous study, where the successful electropolymerization of a bithiophenyl-substituted phthalocyanine compound was described,[80] we explored the possibility for electropolymerizing our target bithiophenyl-containing porphyrin and benzoporphyrin derivatives in this study. The electropolymerization was carried out in $CH_2Cl_2$ containing 0.1 M $TBAPF_6$ and 0.2 mM of the corresponding monomer under the $N_2$ atmosphere by means of the CV. The one-compartment three-electrode cell consisted of the ITO/glass, Ag/AgCl, and the Pt plate as the WE, QRE, and CE, respectively. The potentials ranging from 0.33 to 1.93 V for **ZnP-2** and **ZnP-4**, to 1.83 V for **ZnBP-2**, and to 2.08 V for **ZnBP-4** were applied at the scan rate of 0.05 $V{\cdot}s^{-1}$ for 10 cycles. It should be noted that attempts to electropolymerize the thienyl-substituted porphyrin and benzoporphyrin derivatives failed to give the desirable polymer films possibly because the required potential for the oxidative electropolymerization of their thienyl moieties was higher than that of the bithiophenyl ones and beyond the electrochemical potential window of this study as described in the previous reports.[81,82] The electropolymerization of the bithiophenyl-substituted derivatives was, however, achieved and gave the cyclic voltammograms, as shown in Supporting Information with oxidation peak potentials ($E_{peak,ox}$) observed in the first scan as summarized in Table 2.

The cyclic voltammograms of porphyrins **ZnP-2** (Figure S52) and **ZnP-4** (Figure S53) contained two oxidation peaks in common at 1.22−1.34 V and 1.70−1.84 V, corresponding to the oxidation of the porphyrin core and the bithiophenyl units, respectively.[69] Another peak at 1.19 V was observed for **ZnP-4** and related to the oxidation of its phenyl *meso*-rings.[83] With increasing number of the scanning cycle, the current density of the peaks at 1.22−1.34 V increased and positively shifted, suggesting the possible formation of the polymers of **ZnP-2** (**p-ZnP-2**) and **ZnP-4** (**p-ZnP-4**) that led to the increase in the overall resistance of the polymer-coated electrode. A small broad peak at approximately 0.83 V indicated the oxidation of newly formed oligothiophene.[84] After the polymerization and removal of the excessive monomers with $CH_2Cl_2$, the ITO/glass substrates were found to be coated with pale brown polymer films of **p-ZnP-2** and **p-ZnP-4** (insets of Figures S52


https://doi.org/10.1021/acs.energyfuels.4c01824
Energy Fuels 2024, 38, 16555−16569

and S53) with film thickness and roughness of 54−58 nm and 2.8−5.3 nm, respectively.

As regards the benzoporphyrin series, three oxidation peaks, referring to the oxidation of the $\beta$-benzo fused rings on the porphyrin core, the porphyrin cores, and the bithiophenyl units, were detected at 0.77−0.82 V, 1.01−1.05 V, and 1.60−1.72 V, respectively. In these cases, the oxidation peaks of the newly formed oligothiophene, which should be observed at approximately 0.83 V as mentioned above, might overlap with those of the $\beta$-benzo fused rings and hence could not be clearly seen. This situation also occurred to the peak corresponding to the oxidation of the phenyl *meso*-rings of **ZnBP-4** that appeared in a similar oxidation potential range as the oxidation of the porphyrin core. Upon the increase in the number of the scanning cycles in the electropolymerization process of **ZnBP-2** (Figure S54), the current density increased and the positive shift of the oxidation peaks was observed in the similar manner as the porphyrin series. The resulting polymer film (**p-ZnBP-2**) was found to have a film thickness of 115 nm and a roughness of 12.4 nm. The higher film thickness and roughness of **p-ZnBP-2**, compared with those of **p-ZnP-2** and **p-ZnP-4**, was attributed to larger molecular size and distortion from the planarity of the benzoporphyrin rings.[55] As regards the electropolymerization of **ZnBP-4** on the ITO/glass (Figure S55), the first scanning cycle showed three oxidation peaks at 0.77, 1.01, and 1.72 V, corresponding to the oxidation of the $\beta$-benzo fused ring on the porphyrin core, the porphyrin core, and the bithiophenyl units, respectively. However, no film on the ITO/glass was obtained after the washing process, possibly because the monomer and/or newly formed oligomers of **ZnBP-4** could not strongly attach on the smooth surface of the ITO/glass to grow the polymeric network. Therefore, the electropolymerization was pursued on the carbon paper, where polymer attachment on its high surface area could be enhanced via an $\pi-\pi$ interaction between an $sp^2$ carbon-conjugated network of the benzoporphyrin macrocycles and that of the carbon paper. The polymerization was achieved in DMF containing 0.1 M $TBAPF_6$ and 0.2 mM **ZnBP-4** by applying the potential between 0.33 and 1.83 V with the scan rate of 0.05 $V{\cdot}s^{-1}$ for 10 cycles. The first scanning cycle showed three oxidation peaks at the similar potential ranges as those observed on the ITO/glass, i.e., 0.63, 1.08, and 1.57 V. The slight increase in the current density with the small positive shift of the oxidation peaks observed in the overall cyclic voltammograms suggested the possible formation of the desirable polymer film of **p-ZnBP-4** (Figure S56).

The photophysical properties of the **p-ZnP-2**, **p-ZnP-4**, and **p-ZnBP-2** films on the ITO/glasses were investigated by UV−visible spectrophotometry in comparison with those of their monomer solutions and films. The spectra of all polymer films in Figure 7 exhibited the characteristic Soret and Q-bands at 425−550 nm and 525−700 nm, respectively, which were consistent with those of their monomer solutions and films. Broadening of the absorption bands observed in both polymer and monomer films was generally observed as a result of a higher degree of aggregation of the macrocycles in the bulk films.

**3.5. Preliminary Investigation on Catalytic Performance of p-ZnBP-4 for Heterogeneous Electrochemical Reduction of $CO_2$.** According to the above-mentioned homogeneous experiments, **ZnBP-4** exhibited electrocatalytic activity superior to those of other bithiophenyl-substituted derivatives. Therefore, this study focused on the preliminary

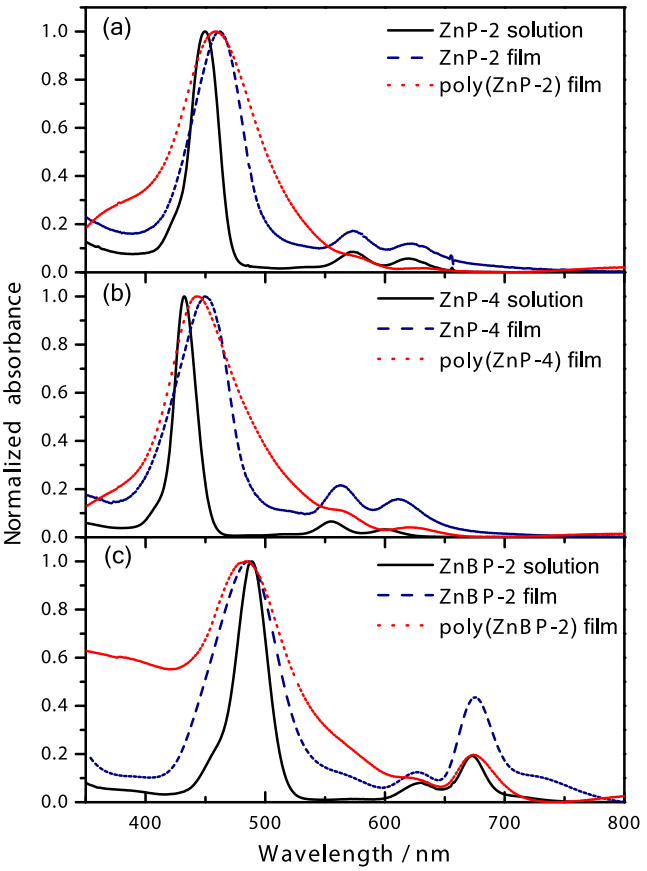


**Figure 7.** Normalized absorption spectra of the monomer solutions (black solid line), the monomer films (blue dashed line), and the polymeric films (red dotted line) of (a) **ZnP-2**, (b) **ZnP-4**, and (c) **ZnBP-2**.

investigation of the electrocatalytic performance of the **p-ZnBP-4** film for heterogeneous reduction of $CO_2$. The experiments were performed in the one-compartment three-electrode cell consisting of a **p-ZnBP-4**-modified carbon paper as the WE, the Pt plate as the CE, and the Ag/AgCl QRE. The cyclic voltammograms were recorded in a 0.1 M $TBAPF_6$ solution in acetonitrile at the potential from 0.33 to −1.57 mV under the $N_2$ and $CO_2$-saturated conditions as shown in Figure 8. Due to the high capacitive current of the pristine carbon paper (Figure S57), the well-resolved reduction features of polymer film could not be obtained under both $N_2$ and $CO_2$-saturated conditions. However, the significant current enhancement was observed at the potential of approximately −1.20 V. Upon the CPE at −1.57 V for 3 h by using the same electrochemical setup, CO was found as the only product with the amount of 0.45 $\mu$mol, corresponding to 5% FE. A current−time plot of this electrolysis showed a stable current at around 0.2 mA observed over the 3-h period, indicating the satisfactory stability of the film (Figure S58). The control experiment by using the bare carbon paper as the WE gave CO with less than 1% FE.

To gain insights into the catalytic activity of **ZnBP-4** in the electrolysis process, the DFT calculation was performed to determine the binding energy of the related intermediates in their lowest-energy adsorption configuration, following an approach described by Chang et al.[85] The calculation suggested that the most stabilized binding site for a $CO_2$ molecule on a **ZnBP-4** saddle-shaped macrocycle was the $Zn^{II}$


https://doi.org/10.1021/acs.energyfuels.4c01824
Energy Fuels 2024, 38, 16555−16569

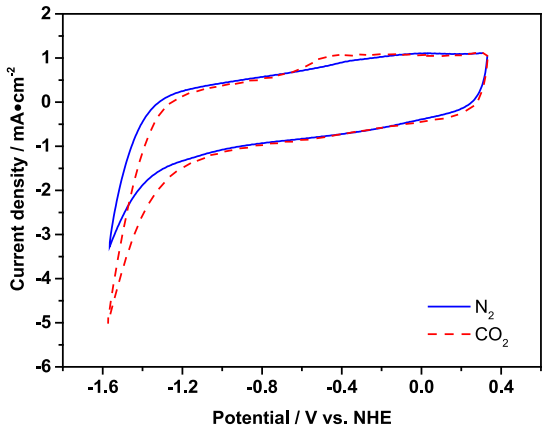


**Figure 8.** Cyclic voltammograms of the **p-ZnBP-4**-coated carbon paper under the $N_2$- (blue solid line) and $CO_2$-saturated conditions (red dashed lines).

center, confirming the metal-centered mechanism rather than the ligand-centered one (Figure S59). As shown in Figure 9, a free energy diagram for the electrochemical $CO_2$ reduction of **ZnBP-4** included 4 states according to reaction coordinates, starting from isolated $CO_2$ and **ZnBP-4** molecules (**S1**), adsorption of HOCO on the **ZnBP-4** molecule (**S2**), desorption of $CO_2$ from the **ZnBP-4** molecule (**S3**), and isolation of free CO and $H_2O$ from the **ZnBP-4** molecule (**S4**). The computed results showed that the formation of *HOCO was a rate-determining step (RDS) with a free energy change of 1.99 eV, corresponding to a previous work.[85] Moreover, weak *HOCO and moderate *CO binding on the $Zn^{II}$ center of **ZnBP-4** suggested that the adsorption of HOCO was quite weak to facilitate electrolysis, while CO desorption was a facile process. This mechanistic consideration provides us guidelines for improving the product yield and the catalytic performance of the benzoporphyrin electrocatalysts via structural modification, namely, altering the metal center and replacing *meso*-phenyl groups of **ZnBP-4** with other functionalized substituents to promote $CO_2$ binding, electrode surface attachment, and the electronic communication with the electrode. Furthermore, film preparation and electrode modification to obtain good film morphology, thickness, and coverage also play important roles in enhancing the catalytic efficiency of the heterogeneous electrocatalysis.

## 4. CONCLUSIONS

Novel $Zn^{II}$-complexes of the *trans*-$A_2B_2$-porphyrin and benzoporphyrin derivatives having 2 phenyl and 2 thiophene-based, i.e., the thienyl or bithiophenyl, *meso*-substituents were successfully synthesized and characterized. The comparison between the porphyrin and benzoporphyrin compounds bearing the same *meso*-substitution patterns revealed that the extension of the $\pi$-conjugated system of the porphyrin core through the $\beta$-fused rings led to the longer absorption and emission maxima but did not significantly affect the electrochemical behavior in the reduction processes. The replacement of the phenyl groups with the thiophene-based units and the addition of one more thiophene ring onto the thienyl groups led to the significant red shift of the absorption and emission maxima, and the positive shift of the reduction peaks in the cyclic voltammograms. Consistently, the theoretical calculation and the crystal structure analysis of **ZnP-3** suggested more efficient electronic communication as a result of the introduction of the $\beta$-fused rings to the macrocycle core and the replacement of the phenyl *meso*-substituents with thiophene-based ones. By means of the CV, the electropolymerization of all bithiophenyl-substituted derivatives to obtain the porphyrin− and benzoporphyrin−oligothiophene conjugated polymer films was achieved. The preliminary CV and CA studies indicated the catalytic activities of the target monomers and the newly prepared **p-ZnBP-4**-modified carbon paper for the homogeneous and heterogeneous electrochemical reduction of $CO_2$ for at least 20 and 3 h, leading to CO formation of up to 9% and 5% FE, respectively. The DFT calculations suggested the metal-centered mechanism with the weak binding energy of the reaction intermediate in the rate-determining step, which could be a reason for the low efficiency of the electrolysis and led to useful guidelines to improve the productivity of the benzoporphyrin-catalyzed electrochemical $CO_2$ reduction for future study.

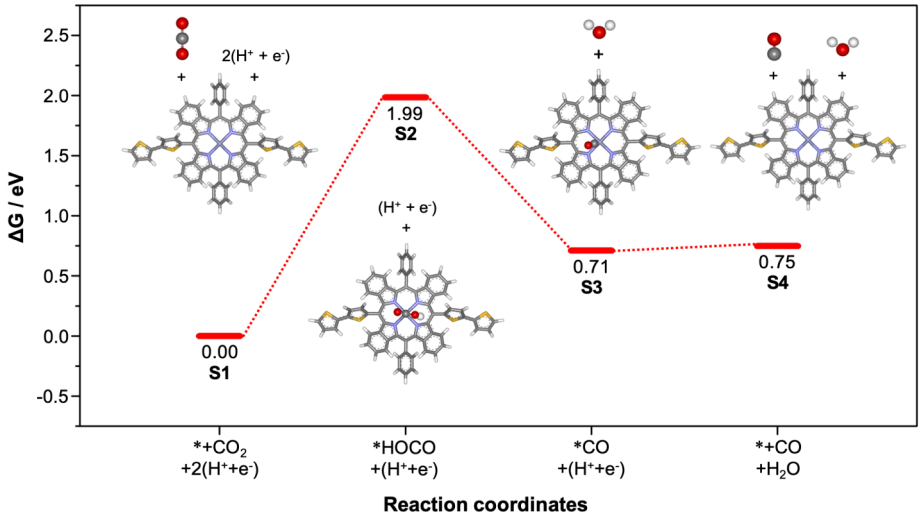


**Figure 9.** Free energy diagram for the electrochemical $CO_2$ reduction of **ZnBP-4**.


https://doi.org/10.1021/acs.energyfuels.4c01824
Energy Fuels 2024, 38, 16555−16569

## ■ ASSOCIATED CONTENT

### Supporting Information

The Supporting Information is available free of charge at https://pubs.acs.org/doi/10.1021/acs.energyfuels.4c01824.

Characterization data of the new compounds, the cyclic voltammograms of the bare carbon-based electrodes and the electropolymerization of the target *trans*-$A_2B_2$ monomers, a chronoamperogram of **p-ZnBP-4** under the $CO_2$-saturated condition, and the most stable structure calculated for $CO_2$ adsorption on **ZnBP-4** (PDF)

## ■ AUTHOR INFORMATION


### Corresponding Author

**P. Thamyongkit** − *Department of Chemistry, Faculty of Science, Chulalongkorn University, Bangkok 10330, Thailand;* orcid.org/0000-0003-0261-3014; Email: patchanita.v@chula.ac.th

### Authors

**H. Seelajaroen** − *Department of Chemistry, Faculty of Science, Chulalongkorn University, Bangkok 10330, Thailand; Linz Institute for Organic Solar Cells (LIOS), Institute of Physical Chemistry Johannes Kepler University Linz, Linz 4040, Austria*

**D. H. Apaydin** − *Linz Institute for Organic Solar Cells (LIOS), Institute of Physical Chemistry Johannes Kepler University Linz, Linz 4040, Austria;* orcid.org/0000-0002-1075-8857

**B. Spingler** − *Department of Chemistry, University of Zurich, Zurich 8057, Switzerland;* orcid.org/0000-0003-3402-2016

**S. Jungsuttiwong** − *Center for Organic Electronic and Alternative Energy, Department of Chemistry and Center of Excellence for Innovation in Chemistry, Faculty of Science, Ubon Ratchathani University, Ubon Ratchathani 34190, Thailand;* orcid.org/0000-0001-5943-6878

**Y. Wongnongwa** − *NSTDA Supercomputer Center (ThaiSC), National Electronics and Computer Technology Center (NECTEC), National Science and Technology Development Agency (NSTDA), Pathum Thani 12120, Thailand*

**R. Rojanathanes** − *Department of Chemistry, Faculty of Science, Chulalongkorn University, Bangkok 10330, Thailand;* orcid.org/0000-0002-0506-3583

**N. S. Sariciftci** − *Linz Institute for Organic Solar Cells (LIOS), Institute of Physical Chemistry Johannes Kepler University Linz, Linz 4040, Austria;* orcid.org/0000-0003-4727-1193

Complete contact information is available at: https://pubs.acs.org/10.1021/acs.energyfuels.4c01824


### Notes

The authors declare no competing financial interest.

## ■ ACKNOWLEDGMENTS

This research was partially supported by the Scholarship from the Graduate School, Chulalongkorn University, to commemorate the 72nd anniversary of his Majesty King Bhumibala Adukadeja; the 90th Anniversary of Chulalongkorn University Fund (Ratchadaphiseksomphot Endowment Fund); and the Thailand Science Research and Innovation Fund Chulalongkorn University. Data collection and composition were supported by funding for high-efficiency postdoc researchers under the Second Century Fund (C2F). The Wittgenstein Prize of Prof. Sariciftci (Solare Energie Umwandlung Z222-N19) is gratefully acknowledged. The authors would like to thank T. Greunz and O. Selyshchev for their valuable suggestion.

## ■ REFERENCES


(1) Aresta, M.; Dibenedetto, A. *In $CO_2$ Conversion and Utilization*; American Chemical Society, 2002; Vol. *809*, pp. 5470.

(2) Kondratenko, E. V.; Mul, G.; Baltrusaitis, J.; Larrazábal, G. O.; Pérez-Ramírez, J. Status and Perspectives of $CO_2$ Conversion into Fuels and Chemicals by Catalytic, Photocatalytic and Electrocatalytic Processes. *Energy Environ. Sci.* **2013**, *6*, 3112−3135.

(3) Aresta, M.; Dibenedetto, A. Utilisation of $CO_2$ as a Chemical Feedstock: Opportunities and Challenges. *Dalton Trans.* **2007**, 2975−2992.

(4) Chueh, W. C.; Haile, S. M. Ceria as a Thermochemical Reaction Medium for Selectively Generating Syngas or Methane from $H_2O$ and $CO_2$. *ChemSuschem* **2009**, *2*, 735−739.

(5) Lehn, J.-M.; Ziessel, R. Photochemical Generation of Carbon Monoxide and Hydrogen by Reduction of Carbon Dioxide and Water under Visible Light Irradiation. *Proc. Natl. Acad. Sci. U. S. A.* **1982**, *79*, 701−704.

(6) Hawecker, J.; Lehn, J.-M.; Ziessel, R. Photochemical and Electrochemical Reduction of Carbon Dioxide to Carbon Monoxide Mediated by (2,2′-Bipyridine)tricarbonylchlororhenium(I) and Related Complexes as Homogeneous Catalysts. *Helv. Chim. Acta* **1986**, *69*, 1990−2012.

(7) Fujita, E. Photochemical Carbon Dioxide Reduction with Metal Complexes. *Coord. Chem. Rev.* **1999**, *185*−*186*, 373−384.

(8) Takeda, H.; Koike; Inoue, H.; Ishitani, O. Development of an Efficient Photocatalytic System for $CO_2$ Reduction Using Rhenium(I) Complexes Based on Mechanistic Studies. *J. Am. Chem. Soc.* **2008**, *130*, 2023−2031.

(9) Fu, Y.; Sun, D.; Chen, Y.; Huang, R.; Ding, Z.; Fu, X.; Li, Z. An Amine-Functionalized Titanium Metal-Organic Framework Photocatalyst with Visible-Light-Induced Activity for $CO_2$ Reduction. *Angew. Chem., Int. Ed.* **2012**, *51*, 3364−3367.

(10) Yu, J.; Low, J.; Xiao, W.; Zhou, P.; Jaroniec, M. Enhanced Photocatalytic $CO_2$-Reduction Activity of Anatase $TiO_2$ by Coexposed {001} and {101} Facets. *J. Am. Chem. Soc.* **2014**, *136*, 8839−8842.

(11) Ishida, H.; Tanaka, K.; Tanaka, T. Electrochemical $CO_2$ Reduction Catalyzed by Ruthenium Complexes $[Ru(Bpy)_2(CO)_2]^{2+}$ and $[Ru(Bpy)_2(CO)Cl]^{+}$. Effect of pH on the Formation of CO and $HCOO^{-}$. *Organometallics* **1987**, *6*, 181−186.

(12) Bhugun, I.; Lexa, D.; Savéant, J.-M. Catalysis of the Electrochemical Reduction of Carbon Dioxide by Iron(0) Porphyrins: Synergystic Effect of Weak Brönsted Acids. *J. Am. Chem. Soc.* **1996**, *118*, 1769−1776.

(13) Dubois, D. L. Development of Molecular Electrocatalysts for $CO_2$ Reduction and $H_2$ Production/Oxidation. *Acc. Chem. Res.* **2009**, *42*, 1974−1982.

(14) Kuhl, K. P.; Cave, E. R.; Abram, D. N.; Jaramillo, T. F. New Insights into the Electrochemical Reduction of Carbon Dioxide on Metallic Copper Surfaces. *Energy Environ. Sci.* **2012**, *5*, 7050−7059.

(15) Lu, Q.; Rosen, J.; Zhou, Y.; Hutchings, G. S.; Kimmel, Y. C.; Chen, J. G.; Jiao, F. A Selective and Efficient Electrocatalyst for Carbon Dioxide Reduction. *Nat. Commun.* **2014**, *5*, 3242.

(16) Lin, S.; Diercks, C. S.; Zhang, Y.-B.; Kornienko, N.; Nichols, E. M.; Zhao, Y.; Paris, A. R.; Kim, D.; Yang, P.; Yaghi, O. M.; et al. Covalent Organic Frameworks Comprising Cobalt Porphyrins for Catalytic $CO_2$ Reduction in Water. *Science* **2015**, *349*, 1208−1213.

(17) Zhang, X.; Wu, Z.; Zhang, X.; Li, L.; Li, Y.; Xu, H.; Li, X.; Yu, X.; Zhang, Z.; Liang, Y.; Wang, H. Highly Selective and Active $CO_2$ Reduction Electrocatalysts Based on Cobalt Phthalocyanine/Carbon Nanotube Hybrid Structures. *Nat. Commun.* **2017**, *8*, 14675.

(18) Benson, E. E.; Kubiak, C. P.; Sathrum, A. J.; Smieja, J. M. Electrocatalytic and Homogeneous Approaches to Conversion of $CO_2$ to Liquid Fuels. *Chem. Soc. Rev.* **2009**, *38*, 89−99.
(19) Kauffman, D. R.; Thakkar, J.; Siva, R.; Matranga, C.; Ohodnicki, P. R.; Zeng, C.; Jin, R. Efficient Electrochemical $CO_2$ Conversion Powered by Renewable Energy. *ACS Appl. Mater. Interfaces* **2015**, *7*, 15626−15632.
(20) Shi, J.; Shen, F.; Shi, F.; Song, N.; Jia, Y. J.; Hu, Y. Q.; Li, Q. Y.; Liu, J.; Chen, T. Y.; Dai, Y. N. Electrochemical reduction of $CO_2$ into CO in tetrabutylammonium perchlorate/ propylene carbonate: water effects and mechanism. *Electrochim. Acta* **2017**, *240*, 114−121.
(21) Kaiser, U.; Heitz, E. Zum Mechanismus der elektrochemischen Dimerisierung von $CO_2$ zu Oxalsäure. *Ber. Bunsenges. Phys. Chem.* **1973**, *77*, 818−823.
(22) Amatore, C.; Savéant, J. M. Mechanism and kinetic characteristics of the electrochemical reduction of carbon dioxide in media of low proton availability. *J. Am. Chem. Soc.* **1981**, *103*, 5021−5023.
(23) Oppel, N.; Röse, P.; Heuser, S.; Prokein, M.; Apfel, U.-P.; Krewer, U. Unveiling the kinetics of $CO_2$ reduction in aprotic electrolyte: The critical role of adsorption. *Electrochim. Acta* **2024**, *490*, 144270.
(24) Kumar, B.; Llorente, M.; Froehlich, J.; Dang, T.; Sathrum, A.; Kubiak, C. P. Photochemical and Photoelectrochemical Reduction of $CO_2$. *Annu. Rev. Phys. Chem.* **2012**, *63*, 541−569.
(25) Azuma, M.; Hashimoto, K.; Hiramoto, M.; Watanabe, M.; Sakata, T. Electrodes in Low-Temperature Aqueous $KHCO_3$ Media. *J. Electrochem. Soc.* **1990**, *137*, 1772−1778.
(26) Noda, H.; Ikeda, S.; Oda, Y.; Imai, K.; Maeda, M.; Ito, K. Electrochemical Reduction of Carbon Dioxide at Various Metal Electrodes in Aqueous Potassium Hydrogen Carbonate Solution. *Bull. Chem. Soc. Jpn.* **1990**, *63*, 2459−2462.
(27) Murata, A.; Hori, Y. Product Selectivity Affected by Cationic Species in Electrochemical Reduction of $CO_2$ and CO at a Cu Electrode. *Bull. Chem. Soc. Jpn.* **1991**, *64*, 123−127.
(28) Hori, Y.; Wakebe, H.; Tsukamoto, T.; Koga, O. Electrocatalytic Process of CO Selectivity in Electrochemical Reduction of $CO_2$ at Metal Electrodes in Aqueous Media. *Electrochim. Acta* **1994**, *39*, 1833−1839.
(29) Ohya, S.; Kaneco, S.; Katsumata, H.; Suzuki, T.; Ohta, K. Electrochemical Reduction of $CO_2$ in Methanol with Aid of CuO and $Cu_2O$. *Catal. Today* **2009**, *148*, 329−334.
(30) Chen, Y.; Kanan, M. W. Tin Oxide Dependence of the $CO_2$ Reduction Efficiency on Tin Electrodes and Enhanced Activity for Tin/Tin Oxide Thin-Film Catalysts. *J. Am. Chem. Soc.* **2012**, *134*, 1986−1989.
(31) Chen, Y.; Li, C. W.; Kanan, M. W. Aqueous $CO_2$ Reduction at Very Low Overpotential on Oxide-Derived Au Nanoparticles. *J. Am. Chem. Soc.* **2012**, *134*, 19969−19972.
(32) Li, C. W.; Kanan, M. W. $CO_2$ Reduction at Low Overpotential on Cu Electrodes Resulting from the Reduction of Thick $Cu_2O$ Films. *J. Am. Chem. Soc.* **2012**, *134*, 7231−7234.
(33) Kas, R.; Kortlever, R.; Milbrat, A.; Koper, M. T. M.; Mul, G.; Baltrusaitis, J. Electrochemical $CO_2$ Reduction on $Cu_2O$-derived Copper Nanoparticles: Controlling the Catalytic Selectivity of Hydrocarbons. *Phys. Chem. Chem. Phys.* **2014**, *16*, 12194−12201.
(34) Xie, J.; Huang, Y.; Yu, H. Tuning the Catalytic Selectivity in Electrochemical $CO_2$ Reduction on Copper Oxide-derived Nanomaterials. *Front Environ. Sci. Eng.* **2015**, *9*, 861−866.
(35) Asadi, M.; Kumar, B.; Behranginia, A.; Rosen, B. A.; Baskin, A.; Repnin, N.; Pisasale, D.; Phillips, P.; Zhu, W.; Haasch, R.; et al. Robust Carbon Dioxide Reduction on Molybdenum Disulphide Edges. *Nat. Commun.* **2014**, *5* (8), 4470.
(36) Chan, K.; Tsai, C.; Hansen Heine, A.; Nørskov, J. K. Molybdenum Sulfides and Selenides as Possible Electrocatalysts for $CO_2$ Reduction. *ChemCatchem* **2014**, *6*, 1899−1905.
(37) Fisher, B. J.; Eisenberg, R. Electrocatalytic Reduction of Carbon Dioxide by Using Macrocycles of Nickel and Cobalt. *J. Am. Chem. Soc.* **1980**, *102*, 7361−7363.
(38) Costentin, C.; Drouet, S.; Robert, M.; Savéant, J.-M. A Local Proton Source Enhances $CO_2$ Electroreduction to CO by a Molecular Fe Catalyst. *Science* **2012**, *338*, 90−94.
(39) Finn, C.; Schnittger, S.; Yellowlees, L. J.; Love, J. B. Molecular Approaches to The Electrochemical Reduction of Carbon Dioxide. *Chem. Commun.* **2012**, *48*, 1392−1399.
(40) Windle, C. D.; Perutz, R. N. Advances in Molecular Photocatalytic and Electrocatalytic $CO_2$ Reduction. *Coord. Chem. Rev.* **2012**, *256*, 2562−2570.
(41) Shen, J.; Kortlever, R.; Kas, R.; Birdja, Y. Y.; Diaz-Morales, O.; Kwon, Y.; Ledezma-Yanez, I.; Schouten, K. J. P.; Mul, G.; Koper, M. T. M. Electrocatalytic Reduction of Carbon Dioxide to Carbon Monoxide and Methane at an Immobilized Cobalt Protoporphyrin. *Nat. Commun.* **2015**, *6* (8), 8177.
(42) Anderson, H. L. Building Molecular Wires from the Colours of Life: Conjugated Porphyrin Oligomers. *Chem. Commun.* **1999**, *23*, 2323−2330.
(43) Takahashi, K.; Hiratsuka, K.; Sasaki, H.; Toshima, S. Electrocatalytic Behavior of Metal Porphyrins in the Reduction of Carbon Dioxide. *Chem. Lett.* **1979**, *8*, 305−308.
(44) Hammouche, M.; Lexa, D.; Savéant, J. M.; Momenteau, M. Catalysis of the Electrochemical Reduction of Carbon Dioxide by Iron("0") Porphyrins. *J. Electroanal Chem. Interfacial Electrochem.* **1988**, *249*, 347−351.
(45) Hammouche, M.; Lexa, D.; Momenteau, M.; Saveant, J. M. Chemical Catalysis of Electrochemical Reactions. Homogeneous Catalysis of the Electrochemical Reduction of Carbon Dioxide by Iron(″0″) Porphyrins. Role of the Addition of Magnesium Cations. *J. Am. Chem. Soc.* **1991**, *113*, 8455−8466.
(46) Bhugun, I.; Lexa, D.; Saveant, J.-M. Carbon Dioxide by an Iron(0) Porphyrin Associated with a Weak Brönsted Acid Cocatalyst. *J. Am. Chem. Soc.* **1994**, *116*, 5015−5016.
(47) Behar, D.; Dhanasekaran, T.; Neta, P.; Hosten, C. M.; Ejeh, D.; Hambright, P.; Fujita, E. Cobalt Porphyrin Catalyzed Reduction of $CO_2$. Radiation Chemical, Photochemical, and Electrochemical Studies. *J. Phys. Chem. A* **1998**, *102*, 2870−2877.
(48) Wu, Y.; Jiang, J.; Weng, Z.; Wang, M.; Broere, D. L. J.; Zhong, Y.; Brudvig, G. W.; Feng, Z.; Wang, H. Electroreduction of $CO_2$ Catalyzed by a Heterogenized Zn-Porphyrin Complex with a Redox-innocent Metal Center. *ACS Cent. Sci.* **2017**, *3*, 847−852.
(49) Dogukan, D. H.; Schlager, S.; Portenkirchner, E.; Sariciftci, N. S. Organic, Organometallic and Bioorganic Catalysts for Electrochemical Reduction of $CO_2$. *ChemPhysChem* **2017**, *18*, 3094−3116.
(50) Windle, C. D.; Reisner, E. Heterogenised Molecular Catalysts for the Reduction of $CO_2$ to Fuels. *Chimia* **2015**, *69*, 435−441.
(51) Portenkirchner, E.; Oppelt, K.; Ulbricht, C.; Egbe, D. A. M.; Neugebauer, H.; Knör, G.; Sariciftci, N. S. Electrocatalytic and Photocatalytic Reduction of Carbon Dioxide to Carbon Monoxide Using the Alkynyl-substituted Rhenium(I) Complex (5,5′-Bisphenylethynyl-2,2′-bipyridyl)$Re(CO)_3Cl$. *J. Organomet. Chem.* **2012**, *716*, 19−25.
(52) Roncali, J. Conjugated Poly(thiophenes): Synthesis, Functionalization, and Applications. *Chem. Rev.* **1992**, *92*, 711−738.
(53) Yamamoto, T. Molecular Assembly and Properties of Polythiophenes. *NPG Asia Mater.* **2010**, *2*, 54−60.
(54) Keawsongsaeng, W.; Gasiorowski, J.; Denk, P.; Oppelt, K.; Apaydin, D. H.; Rojanathanes, R.; Hingerl, K.; Scharber, M.; Sariciftci, N. S.; Thamyongkit, P. Systematic Investigation of Porphyrin-thiophene Conjugates for Ternary Bulk Heterojunction Solar Cells. *Adv. Energy Mater.* **2016**, *6* (11), 1600957.
(55) Solonenko, D.; Gasiorowski, J.; Apaydin, D.; Oppelt, K.; Nuss, M.; Keawsongsaeng, W.; Salvan, G.; Hingerl, K.; Sariciftci, N. S.; Zahn, D. R. T.; et al. Doping-induced Polaron Formation and Solid-state Polymerization in Benzoporphyrin−oligothiophene Conjugated Systems. *J. Phys. Chem. C* **2017**, *121*, 24397−24407.
(56) Sheldrick, G. M. Crystal Structure Refinement with SHELXL. *Acta Crystallogr* **2015**, *C71*, 3−8.
(57) Dolomanov, O. V.; Bourhis, L. J.; Gildea, R. J.; Howard, J. A. K.; Puschmann, H. OLEX2: a Complete Structure Solution,

Refinement and Analysis Program. *J. Appl. Crystallogr.* **2009**, *42*, 339−341.
(58) Spek, A. L. Single-crystal Structure Validation with the Program PLATON. *J. Appl. Crystallogr.* **2003**, *36*, 7−13.
(59) Macrae, C. F.; Bruno, I. J.; Chisholm, J. A.; Edgington, P. R.; McCabe, P.; Pidcock, E.; Rodriguez-Monge, L.; Taylor, R.; van de Streek, J.; Wood, P. A. Mercury CSD 2.0−New Features for the Visualization and Investigation of Crystal Structures. *J. Appl. Crystallogr.* **2008**, *41*, 466−470.
(60) Dolušić, E.; Ngo, H. T.; Maes, W. W.; Dehaen, W. Efficient Synthesis of Aryldipyrromethanes in Water and Their Application in the Synthesis of Corroles and Dipyrromethenes. *Arkivoc* **2007**, *10*, 307−324.
(61) Uppal, T.; Hu, X.; Fronczek, F. R.; Maschek, S.; Bobadova-Parvanova, P.; Vicente, M. G. H. Synthesis, Computational Modeling, and Properties of Benzo-appended Bodipys. *Chem. - Eur. J.* **2012**, *18*, 3893−3905.
(62) Littler, B. J.; Ciringh, Y.; Lindsey, J. S. Investigation of Conditions Giving Minimal Scrambling in the Synthesis of *trans*-Porphyrins from Dipyrromethanes and Aldehydes. *J. Org. Chem.* **1999**, *64*, 2864−2872.
(63) Jiao, J.; Thamyongkit, P.; Schmidt, I.; Lindsey, J. S.; Bocian, D. F. Characterization of Porphyrin Surface Orientation in Monolayers on Au (111) and Si (100) Using Spectroscopically Labeled Molecules. *J. Phys. Chem. C* **2007**, *111*, 12693−12704.
(64) Filatov, M. A.; Lebedev, A. Y.; Vinogradov, S. A.; Cheprakov, A. V. Synthesis of *5*, 15-Diaryltetrabenzoporphyrins. *J. Org. Chem.* **2008**, *73*, 4175−4185.
(65) Filatov, M. A.; Cheprakov, A. V.; Beletskaya, I. P. A Facile and Reliable Method for the Synthesis of Tetrabenzoporphyrin from 4,7-Dihydroisoindole. *Eur. J. Org. Chem.* **2007**, *2007*, 3468−3475.
(66) Finikova, O. S.; Cheprakov, A. V.; Beletskaya, I. P.; Carroll, P. J.; Vinogradov, S. A. Novel Versatile Synthesis of Substituted Tetrabenzoporphyrins. *J. Org. Chem.* **2004**, *69*, 522−535.
(67) Hassel, A. W.; Fushimi, K.; Seo, M. An Agar-based Silver/Silver Chloride Reference Electrode for Use in Micro-electrochemistry. *Electrochem. Commun.* **1999**, *1*, 180−183.
(68) Smith, T. J.; Stevenson, K. J.; Zoski, C. G. *Handbook of Electrochemistry*; Elsevier: Amsterdam, 2007; pp 73−110.
(69) Shimidzu, T.; Segawa, H.; Wu, F.; Nakayama, N. Approaches to Conducting Polymer Devices with Nanostructures: Photoelectrochemical Function of One-dimensional and Two-dimensional Porphyrin Polymers with Oligothienyl Molecular Wire. *J. Photochem. Photobiol. A Chem.* **1995**, *92*, 121−127.
(70) Frisch, M.; Trucks, G.; Schlegel, H.; Scuseria, G.; Robb, M.; Cheeseman, J.; Scalmani, G.; Barone, V.; Petersson, G.; Nakatsuji, H. *GaussView 5.0*; Gaussian, Inc.: Wallingford, CT, 2016.
(71) Lee, C.; Yang, W.; Parr, R. G. Development of the Colle-Salvetti Correlation-Energy Formula into a Functional of the Electron Density. *Phys. Rev. B* **1988**, *37*, 785−789.
(72) Axel, B. *The Quantum Theory of Atoms in Molecules: from Solid State to DNA and Drug Design*; John Wiley & Sons, Ltd, 2007.
(73) Grimme, S.; Antony, J.; Ehrlich, S.; Krieg, H. A Consistent and Accurate Ab Initio Parametrization of Density Functional Dispersion Correction (DFT-D) for the 94 Elements H-Pu. *J. Chem. Phys.* **2010**, *132*, 154104.
(74) Grimme, S.; Ehrlich, S.; Krieg, H. Effect of the Damping Function in Dispersion Corrected Density Functional Theory. *J. Comput. Chem.* **2011**, *32*, 1456−1465.
(75) Shustareva, T. K.; Druzhinina, V. E. Study of Kinetics and Mechanism of Sulfonation of Thiophene and Its Derivatives by Complex Compounds of Sulfuric Anhydride. *Chem. Heterocycl. Compd.* **1986**, *22*, 28−33.
(76) Rochford, J.; Botchway, S.; McGarvey, J. J.; Rooney, A. D.; Pryce, M. T. Photophysical and Electrochemical Properties of *meso*-Substituted Thien-2-yl Zn(II) Porphyrins. *J. Phys. Chem. A* **2008**, *112*, 11611−11618.
(77) Scheidt, W. R.; Kastner, M. E.; Hatano, K. Stereochemistry of the Toluene Solvate of $\alpha,\beta,\gamma,\delta$-Tetraphenylporphinatozinc(II). *Inorg. Chem.* **1978**, *17*, 706−710.
(78) Tawil, S.; Seelajaroen, H.; Petsom, A.; Sariciftci, N. S.; Thamyongkit, P. Clam-shaped Cyclam-functionalized Porphyrin for Electrochemical Reduction of Carbon Dioxide. *J. Porphyrins Phthalocyanines* **2019**, *23*, 453−461.
(79) Apaydin, D. H.; Portenkirchner, E.; Jintanalert, P.; Strauss, M.; Luangchaiyaporn, J.; Sariciftci, N. S.; Thamyongkit, P. Synthesis and Investigation of Tetraphenyltetrabenzoporphyrins for Electrocatalytic Reduction of Carbon Dioxide. *Sustainable Energy Fuels* **2018**, *2*, 2747−2753.
(80) Luangchaiyaporn, J.; Wielend, D.; Solonenko, D.; Seelajaroen, H.; Gasiorowski, J.; Monecke, M.; Salvan, G.; Zahn, D.; Sariciftci, N. S.; Thamyongkit, P. High-performance $Co^{II}$-Phthalocyanine-Based Polymer for Practical Heterogeneous Electrochemical Reduction of Carbon Dioxide. *Electrochim. Acta* **2021**, *367* (12), 137506.
(81) Blanchard, P.; Cravino, A.; Levillain, E. *Handbook of Thiophene-Based Materials*; John Wiley & Sons, Ltd, 2009; pp. 419453.
(82) Diaz, A. F.; Crowley, J.; Bargon, J.; Gardini, G. P.; Torrance, J. B. Electrooxidation of Aromatic Oligomers and Conducting Polymers. *J. Electroanal. Chem.* **1981**, *121*, 355−361.
(83) Denden, Z.; Ezzayani, K.; Saint-Aman, E.; Loiseau, F.; Najmudin, S.; Bonifácio, C.; Daran, J.-C.; Nasri, H. Insights on the UV/Vis, Fluorescence, and Cyclic Voltammetry Properties and the Molecular Structures of $Zn^{II}$ Tetraphenylporphyrin Complexes with Pseudohalide Axial Azido, Cyanato-*N*, Thiocyanato-*N*, and Cyanido Ligands. *Eur. J. Inorg. Chem.* **2015**, *15*, 2596−2610.
(84) Shimidzu, T.; Segawa, H. Porphyrin Arrays Connected with Molecular Wire. *Thin Solid Films* **1996**, *273*, 14−19.
(85) Chang, Q.; Liu, Y.; Lee, J.-H.; Ologunagba, D.; Hwang, S.; Xie, Z.; Kattel, S.; Lee, J. H.; Chen, J. G. Metal-Coordinated Phthalocyanines as Platform Molecules for Understanding Isolated Metal Sites in the Electrochemical Reduction of $CO_2$. *J. Am. Chem. Soc.* **2022**, *144*, 16131−16138.


https://doi.org/10.1021/acs.energyfuels.4c01824
*Energy Fuels* 2024, 38, 16555−16569